

~~CONFIDENTIAL~~

UNCLASSIFIED

NACA

RESEARCH MEMORANDUM

THE STATIC AND DYNAMIC-ROTARY STABILITY DERIVATIVES

AT SUBSONIC SPEEDS OF A MODEL OF THE X-15

RESEARCH AIRPLANE

By Armando E. Lopez and Bruce E. Tinling

Ames Aeronautical Laboratory
Moffett Field, Calif.

CLASSIFICATION CHANGED

UNCLASSIFIED

LIBRARY COPY

SEP 15 1958

LANGLEY AERONAUTICAL LABORATORY
LIBRARY, NACA
LANGLEY FIELD, VIRGINIA

To

By

authority of

TPA #39

CLASSIFIED DOCUMENT

This material contains information affecting the National Defense of the United States within the meaning of the espionage laws, Title 18, U.S.C., Sec. 793 and 794, the transmission or revelation of which in any manner to unauthorized person is prohibited by law.

NATIONAL ADVISORY COMMITTEE
FOR AERONAUTICS

WASHINGTON

September 15, 1958

~~CONFIDENTIAL~~

UNCLASSIFIED

NACA RM A58F09



UNCLASSIFIED

NATIONAL ADVISORY COMMITTEE FOR AERONAUTICS

RESEARCH MEMORANDUM

THE STATIC AND DYNAMIC-ROTARY STABILITY DERIVATIVES

AT SUBSONIC SPEEDS OF A MODEL OF THE X-15

RESEARCH AIRPLANE*

By Armando E. Lopez and Bruce E. Tinling

SUMMARY

Measurements were made in a wind tunnel of the subsonic static and dynamic-rotary stability derivatives of a model of an airplane designed for flight at high supersonic speeds and high altitudes. The model had a low-aspect-ratio wing, a sweptback horizontal tail, and both upper and lower vertical tails.

The effects of flaps and landing gear, speed brakes, and several of the model components are included in the results as well as the stability characteristics of the complete model.

The Mach number range covered in the tests was from 0.22 to 0.92 and the Reynolds numbers were 0.75 and 1.5 million.

INTRODUCTION

The X-15 research airplane, now under construction, is intended to provide flight experience and aerodynamic data at high altitudes and high supersonic speeds. In order to insure adequate predictions of the flying qualities of this airplane, and to aid in the design of the autopilot and the stability augmentation system, a reasonably accurate knowledge of the stability derivatives and control effectiveness is necessary. Because of the unconventional design of the body and vertical-tail surfaces, the values of the stability and control parameters as predicted by existing theories were not considered sufficiently reliable to enable the prediction of the dynamic motions of this airplane.

This report presents the results of measurements obtained in the Ames 12-foot pressure wind tunnel with an 0.09-scale model of the X-15 research

*Title, Unclassified.



UNCLASSIFIED

airplane. Presented herein are the static and the dynamic-stability derivatives throughout the subsonic speed range. The effectiveness of the horizontal tail as a longitudinal control, as well as the effects of landing gear, trailing-edge flaps, speed brakes, and various components of the model on the static and dynamic-stability derivatives, is also included.

NOTATION

The static forces and moments and the damping in pitch have been referred to the stability system of axes (fig. 1). Sufficient data were not available to resolve the measurements of the lateral rotary derivatives to this axes system. These derivatives have been referred to the body system of axes in which the x-axis is coincident with the fuselage reference line.

C_D	drag coefficient, $\frac{\text{drag}}{(1/2)\rho V^2 S}$
C_L	lift coefficient, $\frac{\text{lift}}{(1/2)\rho V^2 S}$
C_Y	side-force coefficient, $\frac{\text{side force}}{(1/2)\rho V^2 S}$
C_l	rolling-moment coefficient, $\frac{\text{rolling moment}}{(1/2)\rho V^2 S b}$
C_m	pitching-moment coefficient, $\frac{\text{pitching moment}}{(1/2)\rho V^2 S \bar{c}}$
C_n	yawing-moment coefficient, $\frac{\text{yawing moment}}{(1/2)\rho V^2 S b}$
M	Mach number
R	Reynolds number, based on mean aerodynamic chord
S	wing area
V	velocity
b	wing span
\bar{c}	wing mean aerodynamic chord
p	rolling velocity
q	pitching velocity

r	yawing velocity
t	time
α	angle of attack
α_u	angle of attack, uncorrected for tunnel wall interference
β	angle of sideslip
δ_f	angle of flap deflection
δ_h	angle of incidence of the horizontal tail
δ_s	angle of deflection of speed brakes
ρ	air density
$(\dot{})$	$\frac{d()}{dt}$
$()'$	() referred to body axes

Subscripts

L	lower speed brakes
U	upper speed brakes
ex	extended speed brakes (see fig. 2(b))

The various stability derivatives are defined as follows:

$C_{m_q}, C_{m_{\dot{\alpha}}}$	derivatives with respect to $\left(\frac{c}{2V}\right)$ times subscript
$C_{l_p}, C_{l_r}, C_{l_\beta}$ $C_{n_p}, C_{n_r}, C_{n_\beta}$	derivatives with respect to $\left(\frac{b}{2V}\right)$ times subscript
$\frac{C_Y}{\beta}$	$\frac{(C_Y)_{\Delta\beta=0}}{\beta^0}$
$\frac{C_l}{\beta}$	$\frac{(C_l)_{\Delta\beta=0}}{\beta^0}$
$\frac{C_n}{\beta}$	$\frac{(C_n)_{\Delta\beta=0}}{\beta^0}$

MODEL AND APPARATUS

The 0.09-scale model of the X-15 research airplane was supplied by North American Aviation Company, Inc. Drawings and photographs showing the model and the method of supporting it in the wind tunnel are presented in figures 2 and 3. The pertinent geometric parameters and model dimensions are presented in table I.

It is desirable that models used for dynamic stability tests be as light as possible. For the model of these tests, light weight was achieved by machining the aerodynamic surfaces and supporting structure from magnesium forgings. The fuselage was formed from laminated Fiberglas. The total weight of the model was about 16 pounds.

The two lower vertical tails shown in figure 2 were tested. The larger of these represents the configuration for the major portion of the flight, and the shorter one represents the configuration for approach and landing.

It can also be seen from figure 2, that two fuselage shapes were used; one in which the side fairings originated near the nose and one in which the fairings originated near the canopy.

The static forces and moments were measured on a 2-1/2-inch diameter, six-component, internal, strain-gage balance. Measurements of the rotary derivatives were made with a single-degree-of-freedom oscillation system in which the derivatives due to pitching velocity and to yawing velocity about the body system of axes are measured directly. The derivatives due to rolling velocity, however, are measured in a combined rolling and yawing oscillation about an inclined axis and are then separated algebraically. The apparatus and technique for obtaining the various derivatives are described in detail in reference 1.

CORRECTIONS TO DATA

The data were corrected by the method of reference 2 for the induced effects of the wind-tunnel walls resulting from lift on the model. The magnitude of the corrections which were added to the measured values are:

$$\Delta\alpha = 0.11 C_L$$

$$\Delta C_D = 0.0019 C_L^2$$

The induced effects of the tunnel walls on the pitching moments were calculated and found to be negligible.

The Mach number and dynamic pressure were corrected for the constriction due to the wind-tunnel walls by the method of reference 3. At a Mach number of 0.94, this correction amounted to an increase of about 1 percent in the measured Mach number and dynamic pressure.

The drag data have been adjusted to correspond to a base pressure equal to free-stream static pressure.

The measured values of damping moments were corrected for internal damping of the model and apparatus. This internal or frictional damping was determined from measurements with the wind off and the tunnel evacuated to various pressures below atmospheric. These measured moments were extrapolated to zero pressure and the extrapolated values subtracted from the data.

The effect of resonance due to the presence of tunnel walls on the measured values of damping cannot be accurately determined. Calculations based on the method of reference 4, however, indicate a minimum wind-tunnel resonant frequency of about 17 cycles per second. Since the oscillation frequency never exceeded 9 cycles per second, it is doubtful that resonance due to the wind-tunnel walls had any important effect on the data.

TESTS

Unless otherwise stated, all the data were obtained with a horizontal-tail deflection angle of $-2-1/2^\circ$ and at a Reynolds number of 1.5 million.

During the interval between the dynamic stability tests and the static force tests, the fuselage shape was changed. For the dynamic stability measurements the side fairings originated near the nose of the fuselage, and for the static force tests the side fairings originated near the canopy.

The derivatives due to rolling velocity could not be measured throughout the Mach number range, primarily because of the technique employed.

The system involved measurement of the components of all lateral-directional derivatives simultaneously during a single-degree-of-freedom oscillation about an inclined axis. The rolling derivatives were then separated by subtraction of the yawing derivatives which were measured directly. For the model of this test, the damping in yaw was approximately five times the magnitude of the next largest lateral-rotary stability derivative. Consequently, a small percentage error in the measurement would result in a large percentage error in the rolling derivative. The only reliable measurements of the rolling derivatives were obtained at a Mach number of 0.22.

During the dynamic stability tests with the speed brakes deflected, the model experienced severe random disturbances, making it virtually impossible to obtain data at a Reynolds number of 1.5 million at Mach numbers above 0.22. In order to reduce the intensity of these random disturbances the Reynolds number was reduced to 0.75 million for the dynamic stability tests for the model with the speed brakes.

RESULTS

The results of the wind-tunnel tests are presented in the following figures:

	<u>Figure</u>
Static longitudinal characteristics	
Complete model with several tail incidences	4
Effect of speed brakes	5
Effect of flaps and landing gear	6
Effect of fuselage shape	7
Damping in pitch	8
Effects of Mach number on the longitudinal stability parameters	9
Static lateral-directional stability characteristics	
Variation of lateral-directional coefficients with sideslip	10
Variation of lateral-directional coefficients with angle of attack	11
Separate effects of speed brakes	12
Lateral-directional rotary stability derivatives	
Complete model and several vertical tail configurations	13
Effects of speed brakes	14
Effects of flaps and landing gear	15
Effects of Mach number on the lateral-directional derivatives	16

Summary of Results

Static longitudinal stability.- The static longitudinal stability increased with increasing angle of attack from a region of instability at negative angles of attack to a static margin as large as 40 percent of the mean aerodynamic chord at the higher angles of attack (fig. 4). This variation resulted mainly from a change in horizontal-tail contribution with angle of attack. The effectiveness of the tail as a longitudinal control, however, remained nearly constant throughout the angle-of-attack range.

Deflection of the speed brakes resulted in a reduction in stability and a nose-down increment in pitching moment at lift coefficients below 0.4 (see fig. 5).

A trailing-edge flap deflection of 40° and extension of the landing gear caused a nose-up moment sufficient to increase the trimmed lift coefficient for a horizontal-tail deflection angle of 0° by about 0.6 (see fig. 6).

The fuselage shape was found to have a pronounced effect on stability as is shown in figure 7. When the side fairings originated near the nose, rather than near the canopy, the complete model was longitudinally unstable at angles of attack greater than 15° .

Damping in pitch.- The value of $C_{m_q} + C_{m_{\dot{\alpha}}}$ for the complete model varied from about -10 at a Mach number of 0.22 to about -17 at a Mach number of 0.92 (figs. 8 and 9). The wing-fuselage combination contributed about 30 percent of the total damping moment. In general, deflection of the speed brakes or deflection of the flaps and landing gear had no important effects on the damping in pitch.

Static lateral stability.- The complete model was directionally stable and had a slight negative effective dihedral throughout the Mach number range at zero angle of attack (see fig. 11). The directional stability, however, diminished markedly as the angle of attack was increased beyond 8° to 10° . Removing the lower part of the lower vertical tail reduced the directional stability by approximately one-third at low angles of attack and resulted in directional instability near 17° . As would be expected removal of part of the lower vertical tail resulted in a positive increment to the effective dihedral and generally resulted in positive effective dihedral for the landing configuration at all positive angles of attack.

Deflecting the speed brakes resulted in a reduction in directional stability at angles of attack greater than 6° . For the complete models, deflecting the speed brakes resulted in directional instability at 15° angle of attack (fig. 12).

Lateral-directional rotary stability derivatives.- The damping-in-yaw coefficient for the complete model varied from about -1.2 at a Mach number of 0.22 to about -1.7 at a Mach number of 0.90. A further increase in Mach number to 0.94 resulted in a slight reduction in damping in yaw (fig. 13). The rolling moment due to yawing velocity, $C_{l_r} - C_{l_{\dot{\beta}}} \cos \alpha$, generally had a positive trend with angles of attack above about 6° .

Deflection of the speed brakes (fig. 14) caused a large reduction in damping in yaw at low angles of attack and caused large variations throughout the angle-of-attack range. Extending the speed brakes laterally so that a gap existed between the brakes and the vertical-tail surfaces, as shown in figure 2(b), reduced the destabilizing tendencies at Mach numbers below 0.90. No benefit was experienced at a Mach number of 0.90 and the extended speed-brake configuration appeared somewhat more destabilizing at a Mach number of 0.92.

Deflection of the flaps and landing gear had no important effects on the derivatives due to yawing velocity at a Mach number of 0.22 (fig. 15).

As noted previously it was impossible to measure the derivatives due to rolling velocity throughout the Mach number range. The data which were obtained at a Mach number of 0.22 are shown in figure 15 with and without landing gear and flap deflections. For the complete model these data indicate a damping-in-roll coefficient of about -0.3 and a yawing moment due to rolling velocity of essentially zero throughout the angle-of-attack range.

Ames Aeronautical Laboratory
National Advisory Committee for Aeronautics
Moffett Field, Calif., June 9, 1958

REFERENCES

1. Beam, Benjamin H.: A Wind-Tunnel Test Technique for Measuring the Dynamic Rotary Stability Derivatives at Subsonic and Supersonic Speeds. NACA Rep. 1258, 1956. (Supersedes NACA TN 3347)
2. Glauert, H.: Ch. XIV, The Elements of Aerofoil and Airscrew Theory. The University Press, Cambridge, England, 1926.
3. Herriot, John G.: Blockage Corrections for Three-Dimensional-Flow Closed-Throat Wind Tunnels With Consideration of the Effects of Compressibility. NACA Rep. 995, 1950. (Supersedes NACA RM A7B28)
4. Runyan, Harry L., Woolston, Donald S., and Rainey, A. Gerald: Theoretical and Experimental Investigation of the Effects of Tunnel Walls on the Forces on an Oscillating Airfoil in Two Dimensional Subsonic Compressible Flow. NACA TN 3416, 1955.

TABLE I.- MODEL GEOMETRY

Wing (leading and trailing edges extended to body center line)	
Aspect ratio	2.5
Taper ratio	0.20
Sweepback, leading edge, deg	36.75
Root chord, ft	1.342
Tip chord, ft	0.268
Dihedral, deg	0
Incidence, deg	0
Twist, deg	0
Airfoil section	NACA 66 series (mod)
Thickness ratio	0.0445
Area, sq ft	1.620
Span, ft	2.012
Mean aerodynamic chord, ft	0.924
Horizontal tail (leading and trailing edges extended to body center line and projected to wing chord plane)	
Aspect ratio	2.92
Taper ratio	0.206
Sweepback, c/4, deg	45
Root chord, ft	0.920
Tip chord, ft	0.190
Dihedral, deg	-15
Twist, deg	0
Airfoil section	NACA 66 series (mod)
Thickness ratio	0.05
Area, sq ft	0.903
Span, ft	1.626
Mean aerodynamic chord, ft	0.635
Length (moment center to $\bar{c}/2$ of the tail), ft	1.221
Upper vertical tail (leading and trailing edges extended to wing chord plane)	
Taper ratio	0.655
Sweepback, leading edge, deg	30
Airfoil section	10° single wedge
Root chord, ft	1.039
Tip chord, ft	0.681
Area, sq ft	0.535
Span, ft	0.622

TABLE I.- MODEL GEOMETRY - Concluded

Lower vertical tails (leading and trailing edges extended to wing chord plane)		
	Large	Small
Taper ratio	0.693	0.811
Sweepback of leading edge, deg	30	30
Airfoil section	10° single wedge	
Root chord, ft	1.039	1.039
Tip chord, ft	0.720	0.843
Area, sq ft	0.481	0.322
Span, ft	0.547	0.342
Body		
Length, ft		4.425
Base area, sq ft		0.101
Moment center (on body center line)		
Horizontal location, percent \bar{c}		25

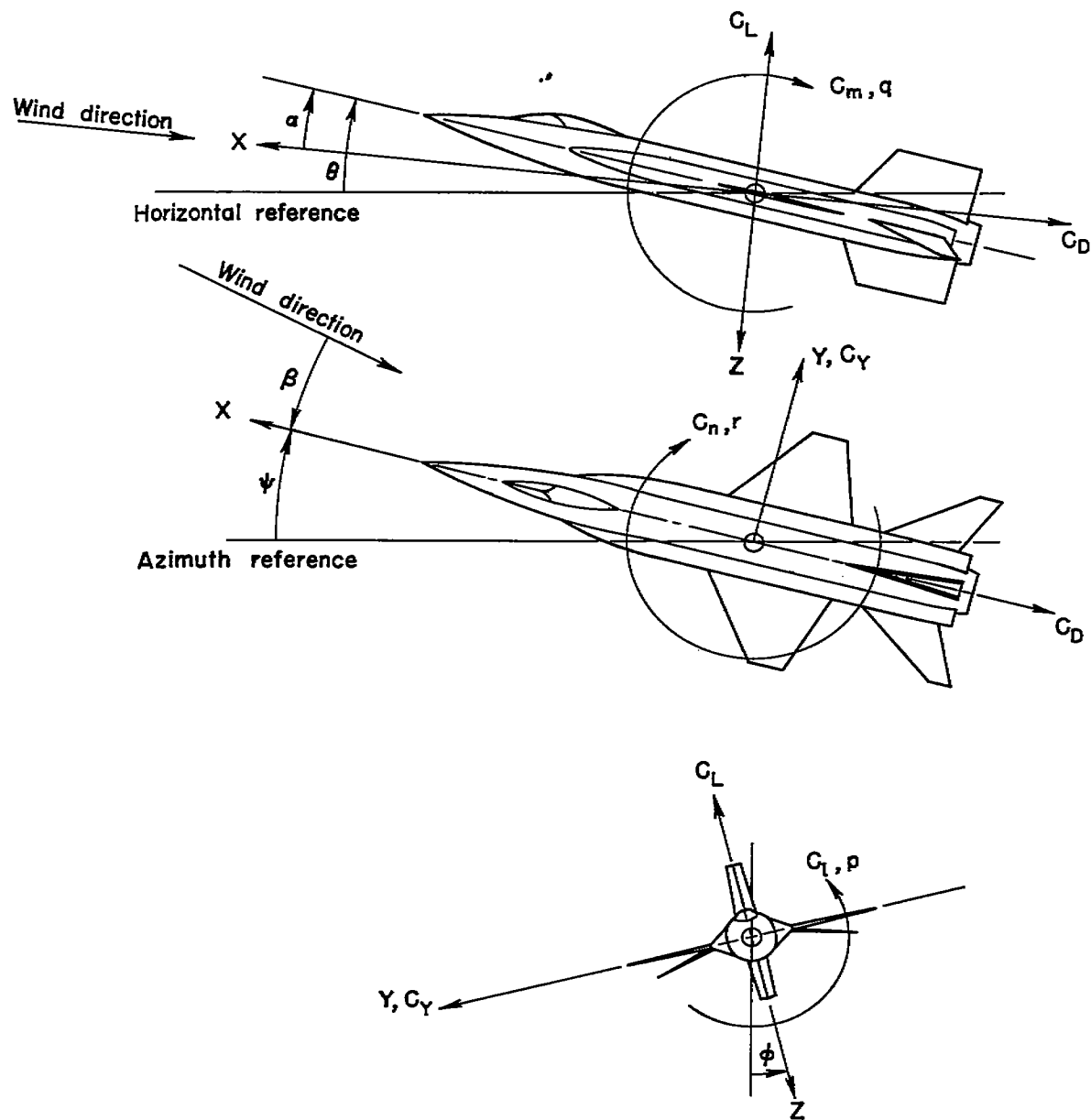
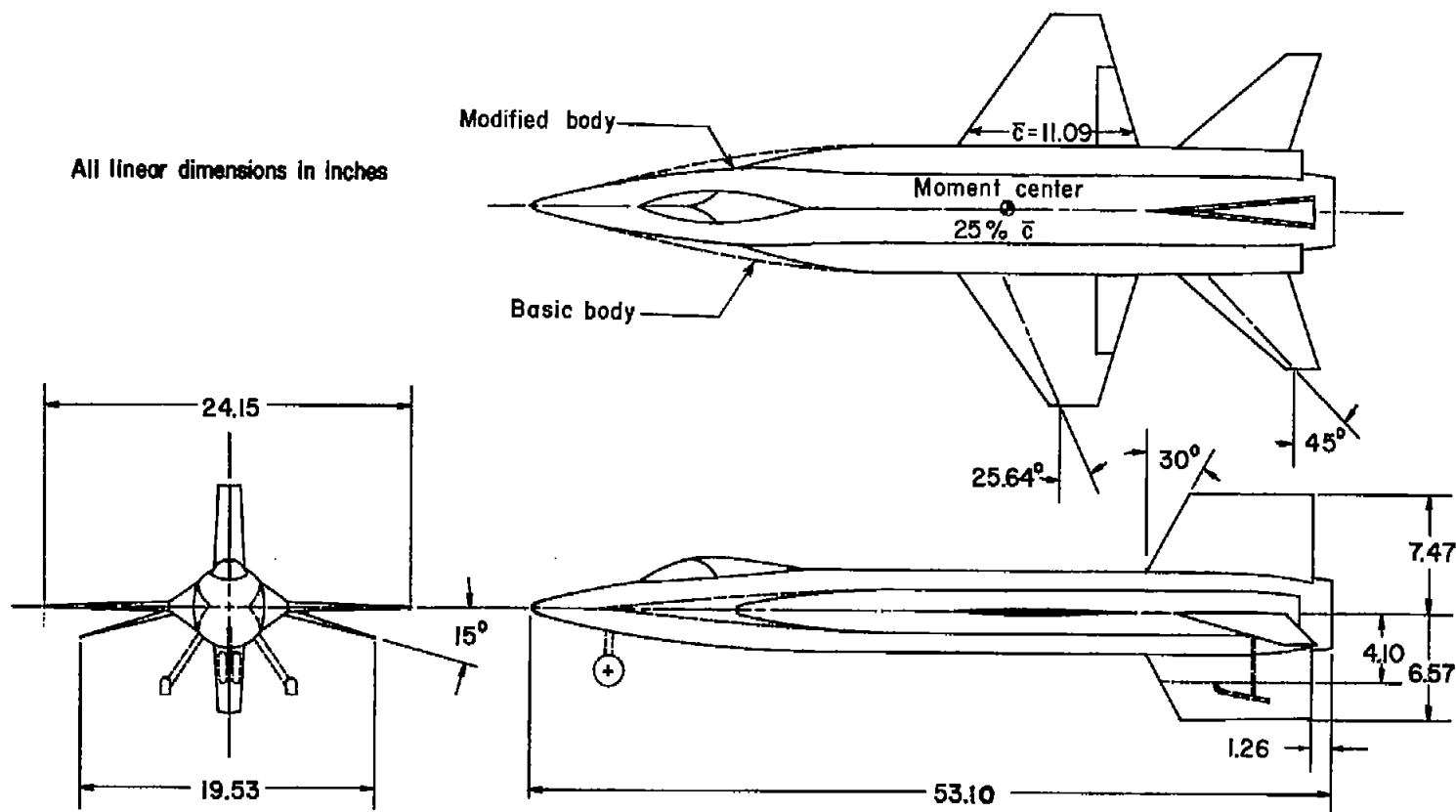
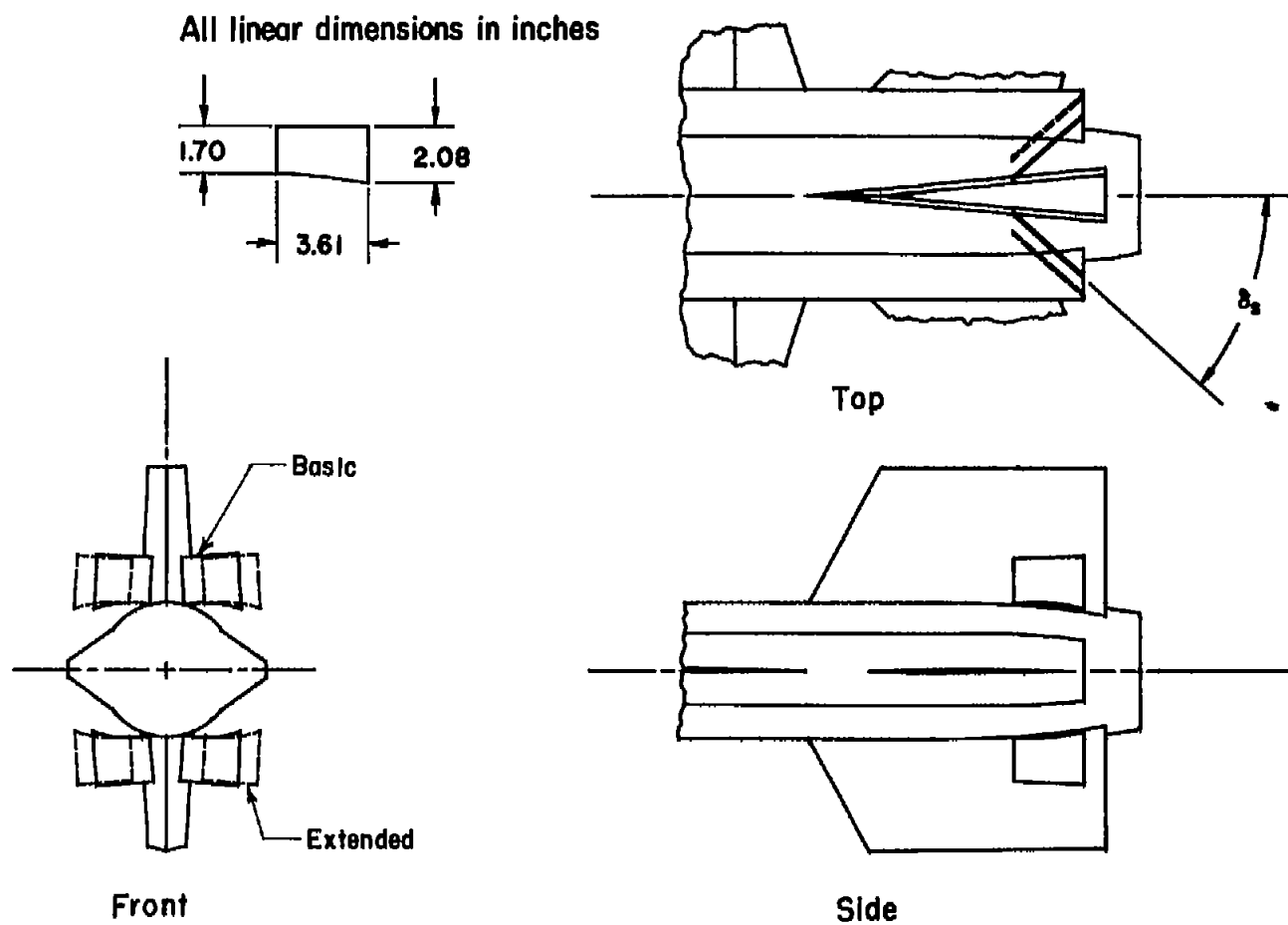


Figure 1.- The stability system of axes.



(a) Three-view drawing.

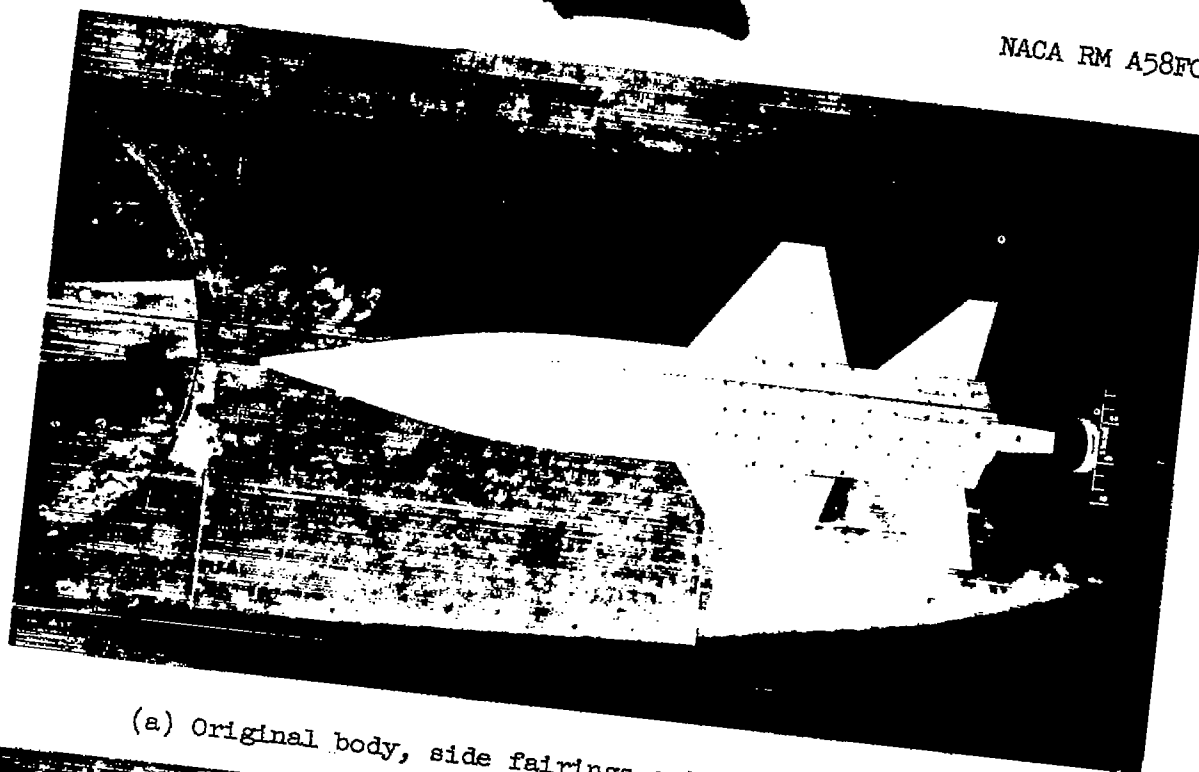
Figure 2.- Model dimensions.



(b) Speed-brake details.

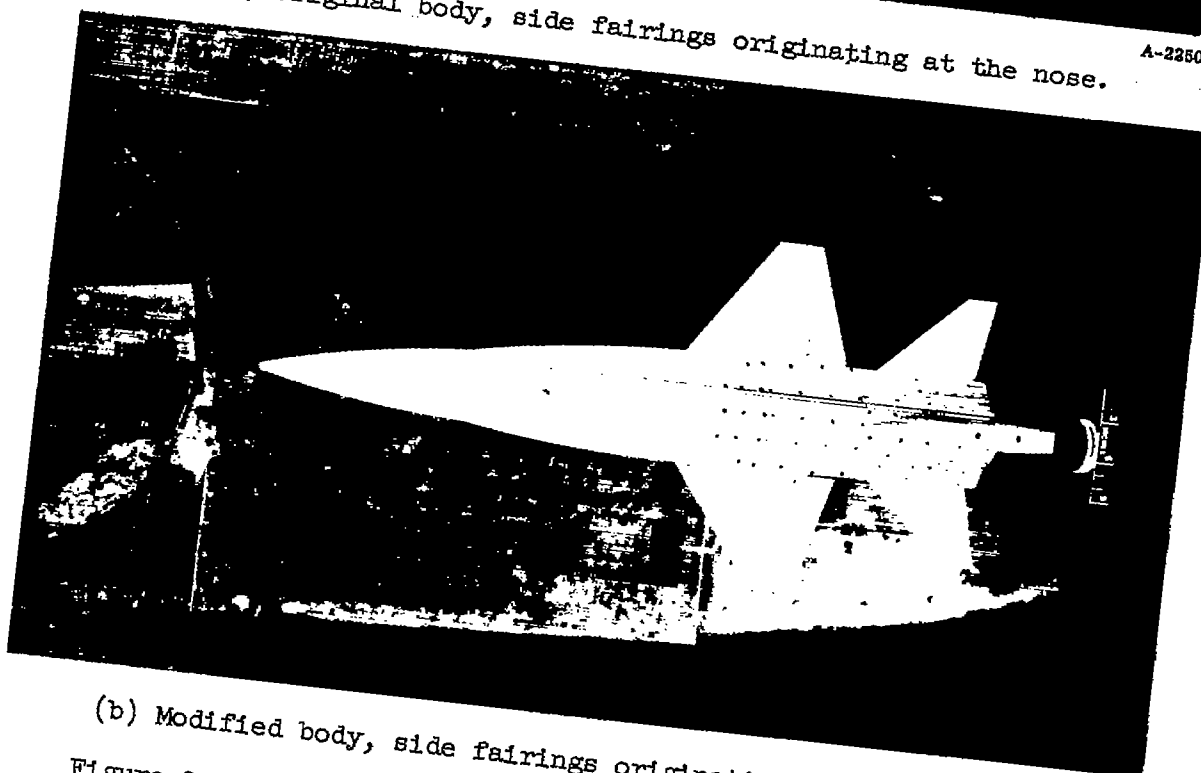
Figure 2.- Concluded.

NACA RM A58F09



(a) Original body, side fairings originating at the nose.

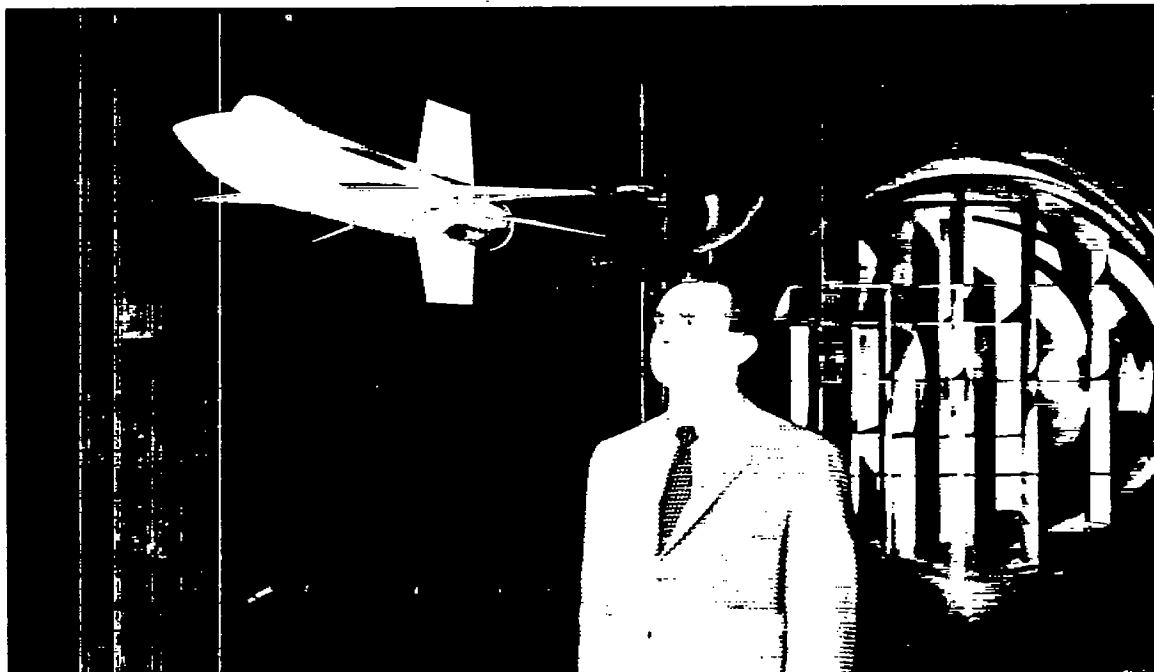
A-22507



(b) Modified body, side fairings originating near the canopy.

A-22506

Figure 3.- Photographs of the model mounted in the wind tunnel.



(c) Three-quarter front view.

A-22504

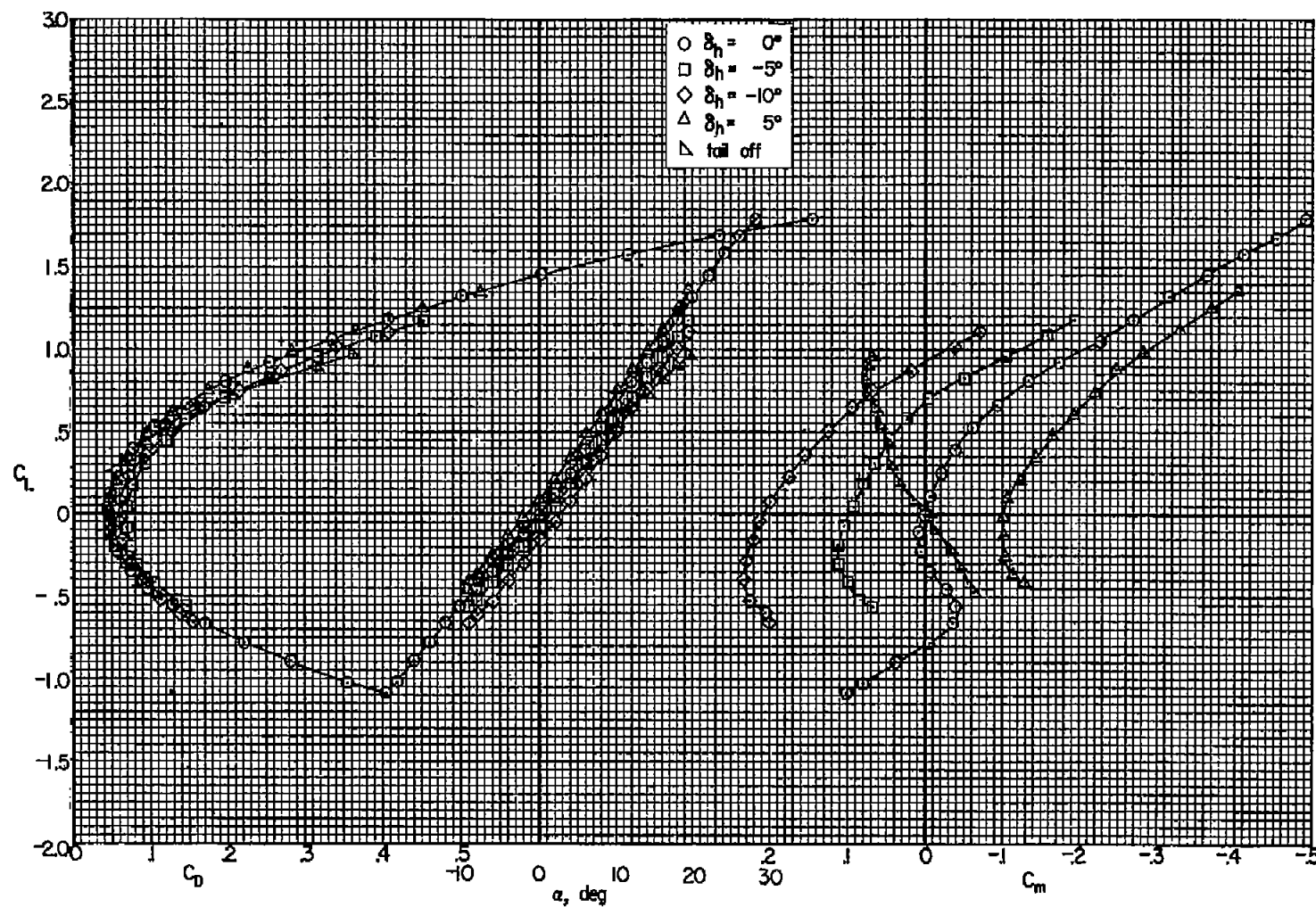


(d) Three-quarter rear view.

A-22505

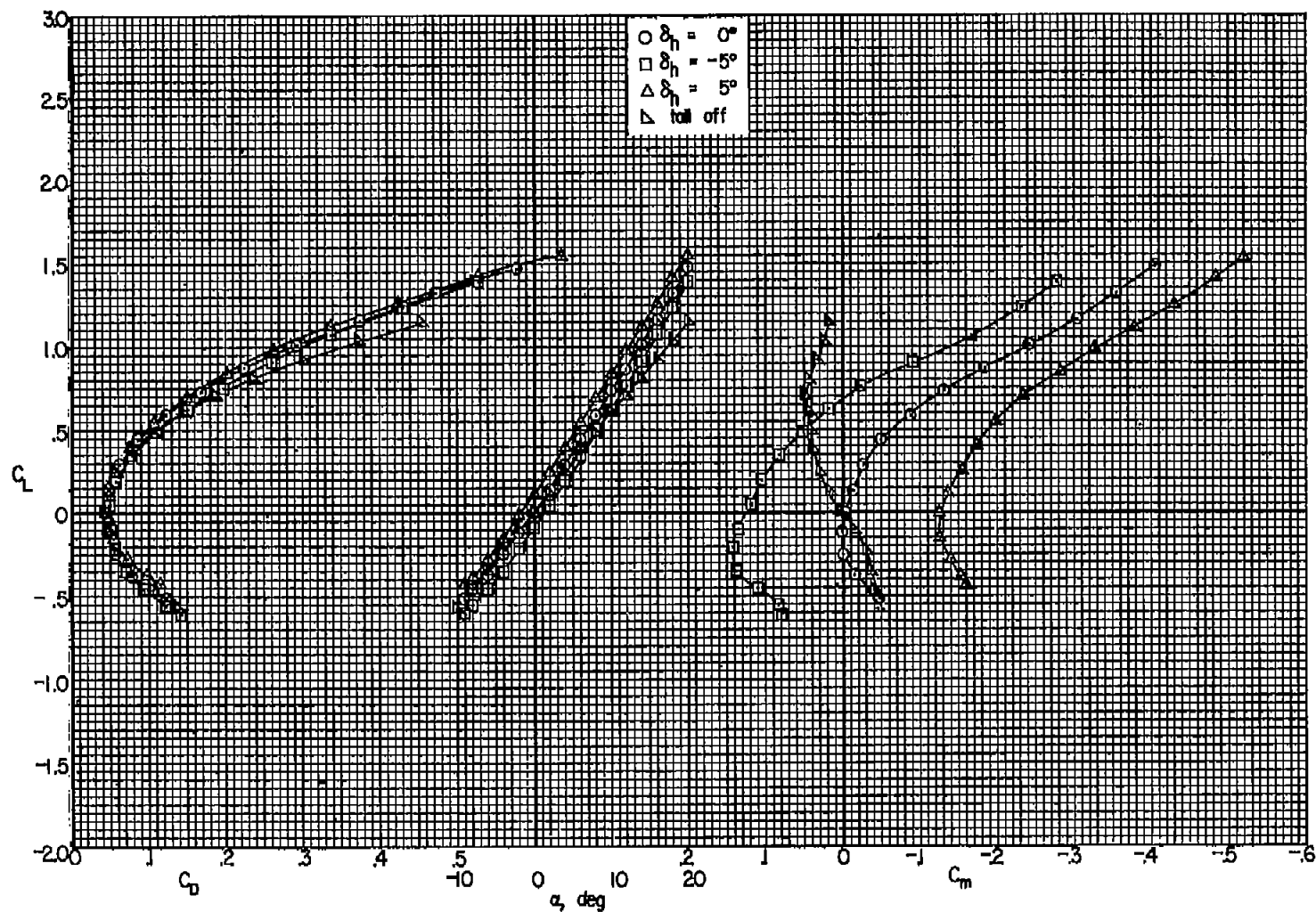
Figure 3.- Concluded.





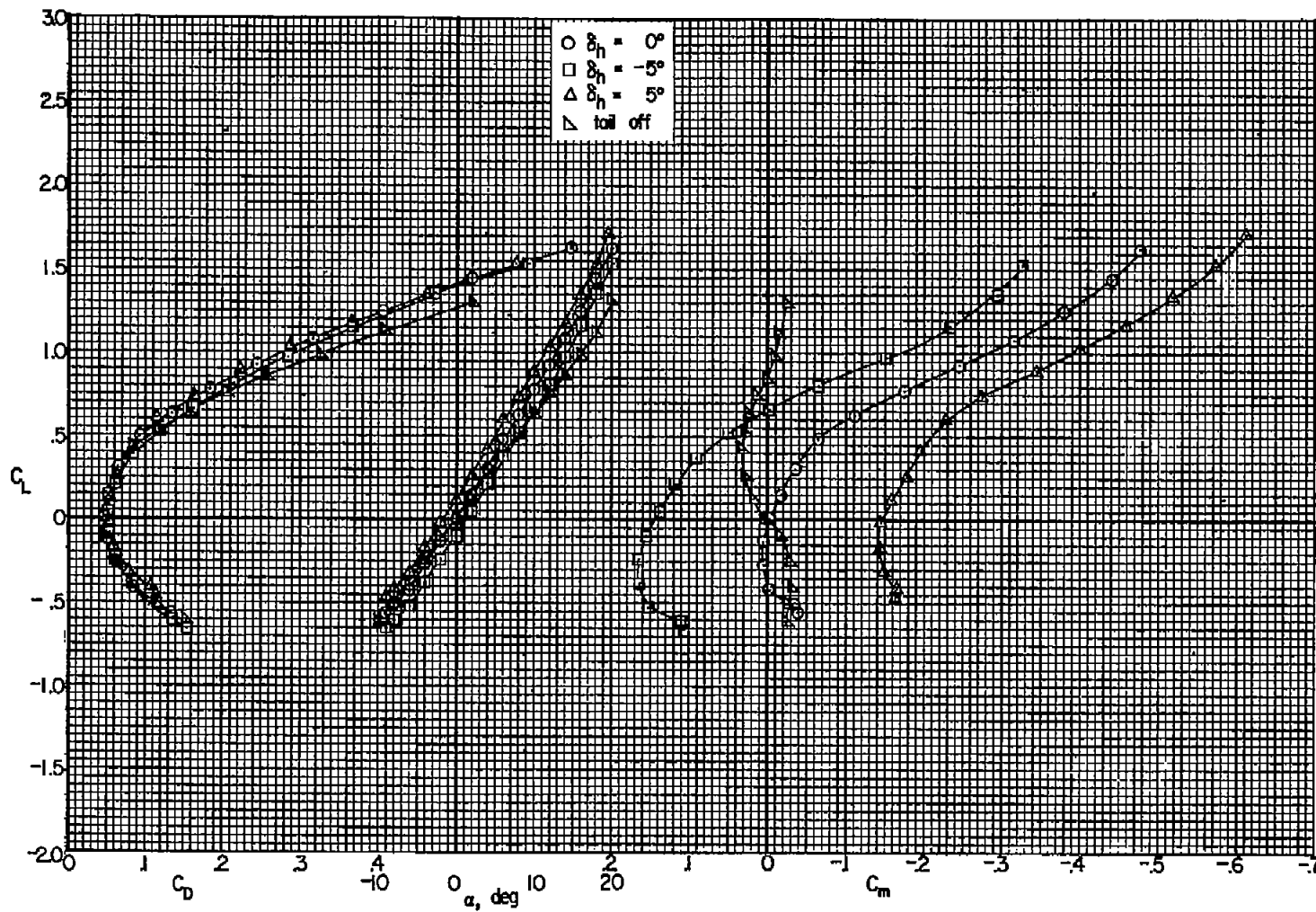
(a) $M = 0.22$

Figure 4.- Lift, drag, and pitching-moment coefficients; wing, modified body, empennage.



(b) $M = 0.80$

Figure 4.- Continued.



(c) $M = 0.90$

Figure 4.- Continued.

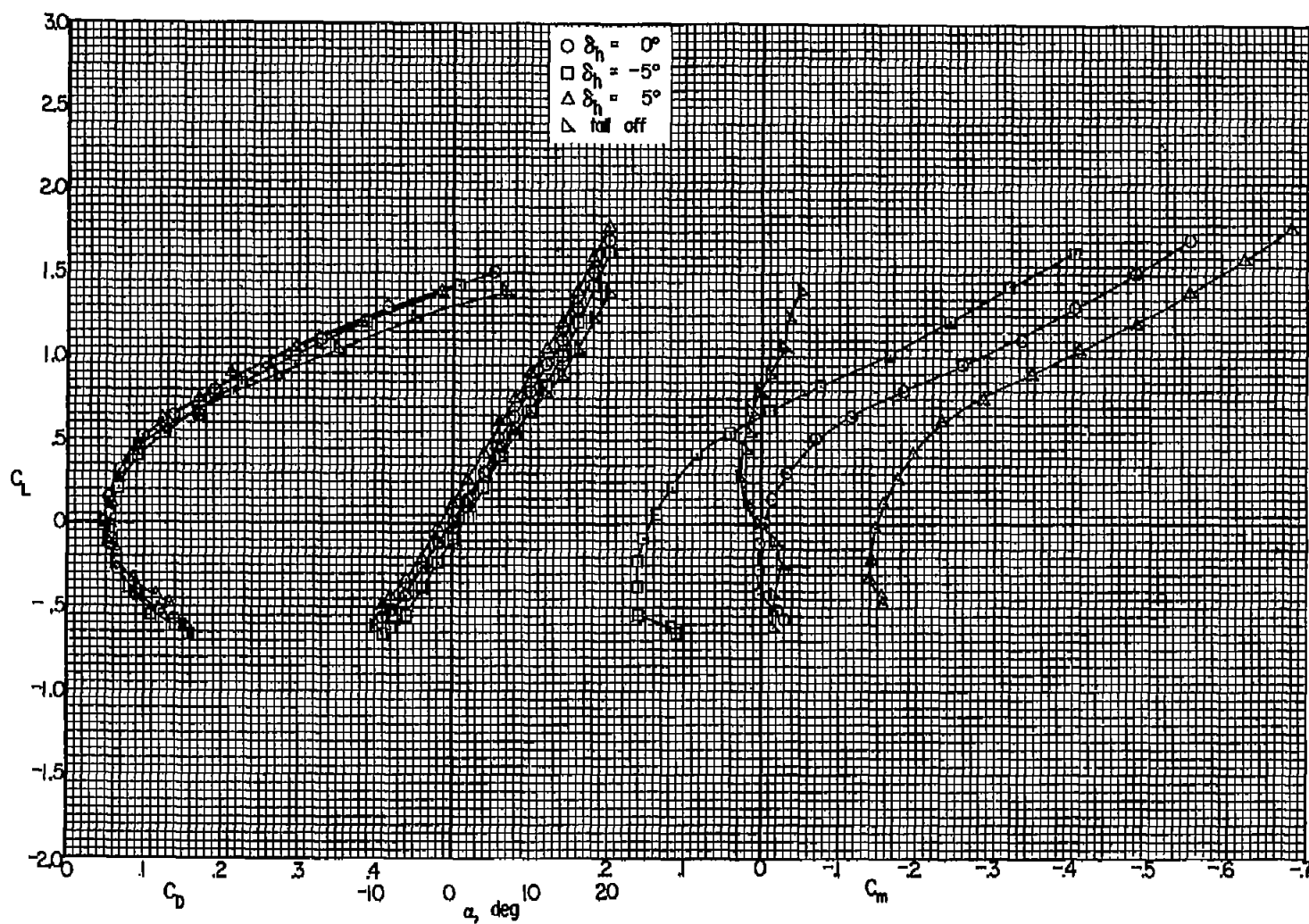
(d) $M = 0.92$

Figure 4.- Concluded

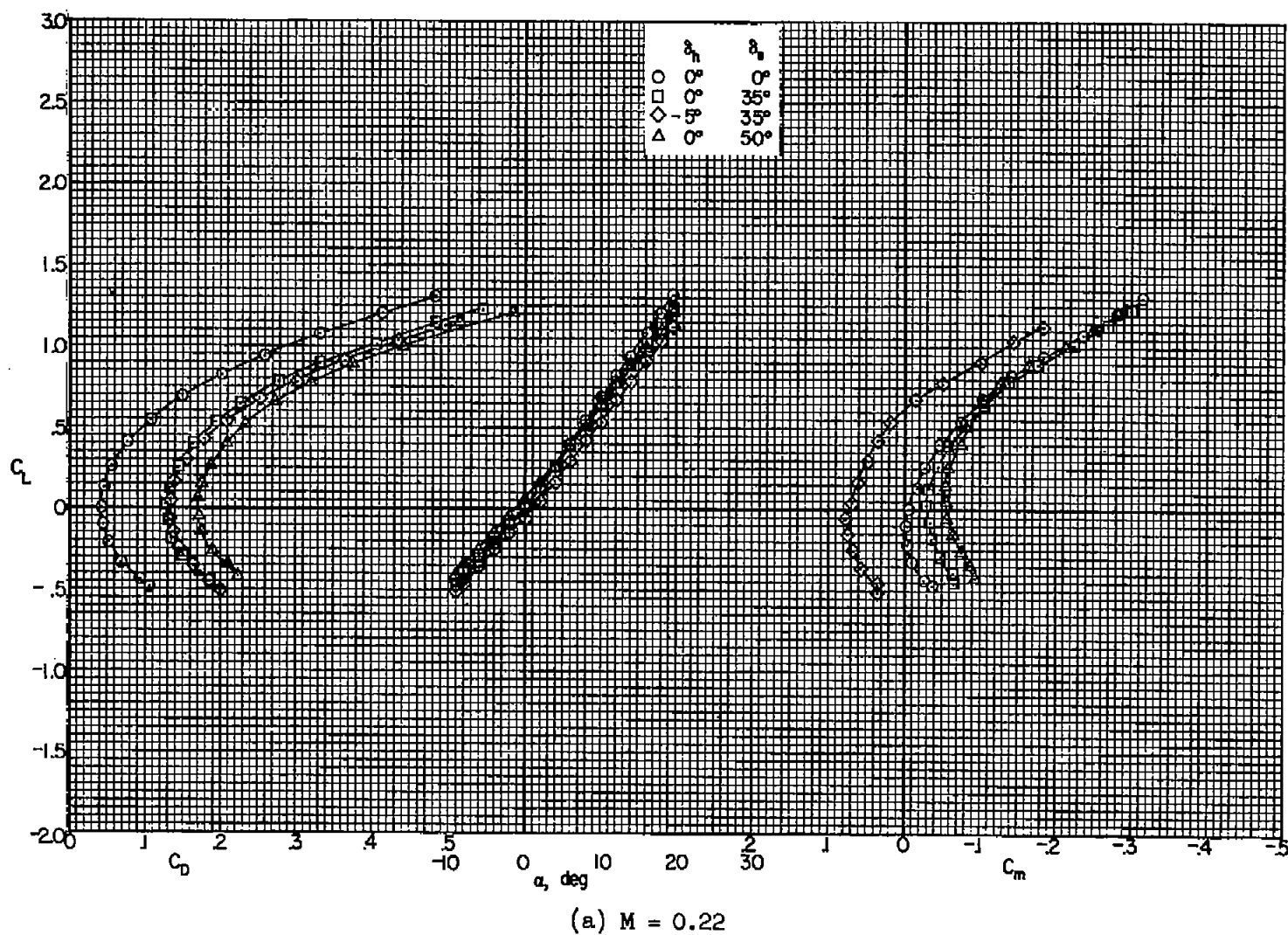
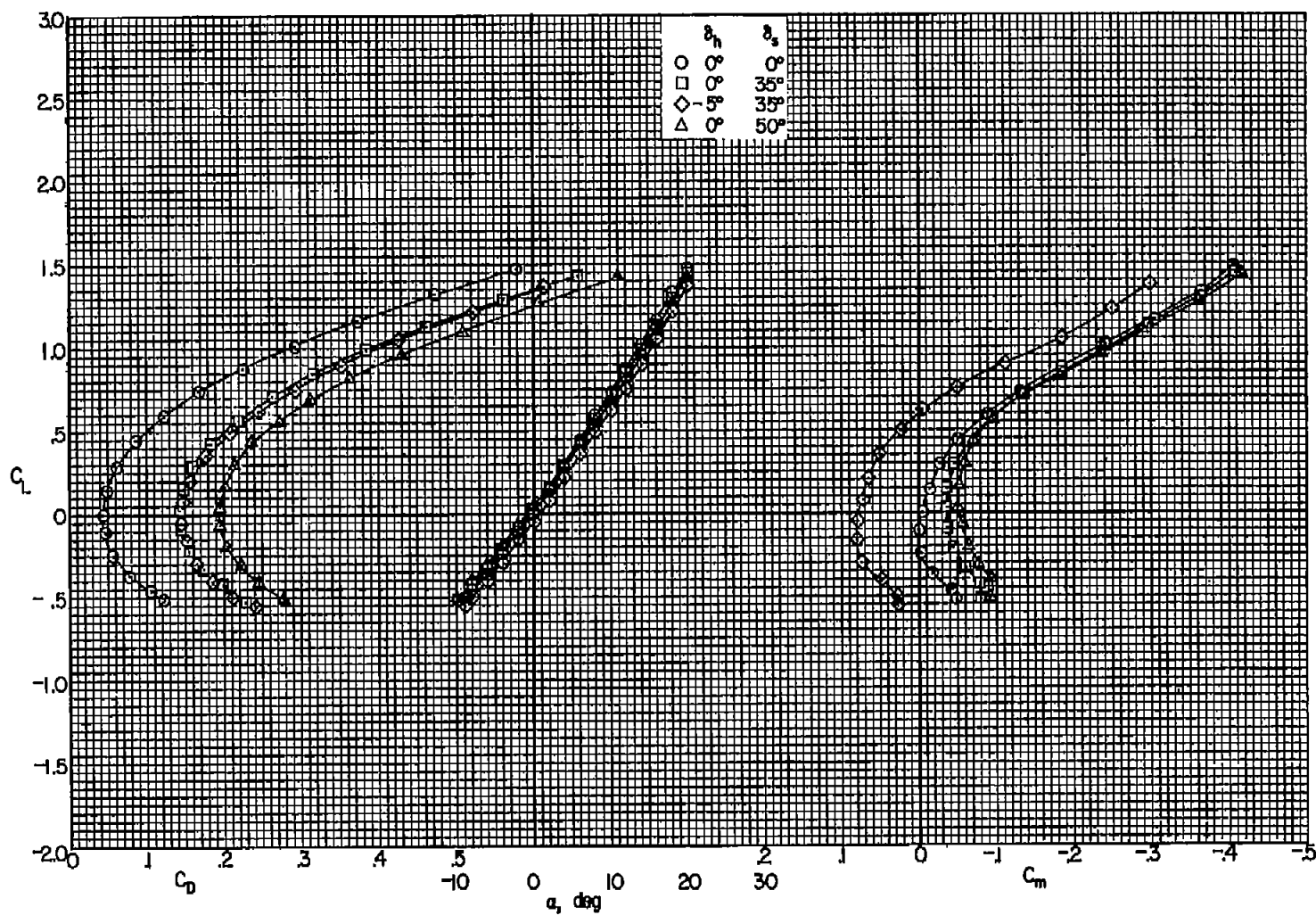
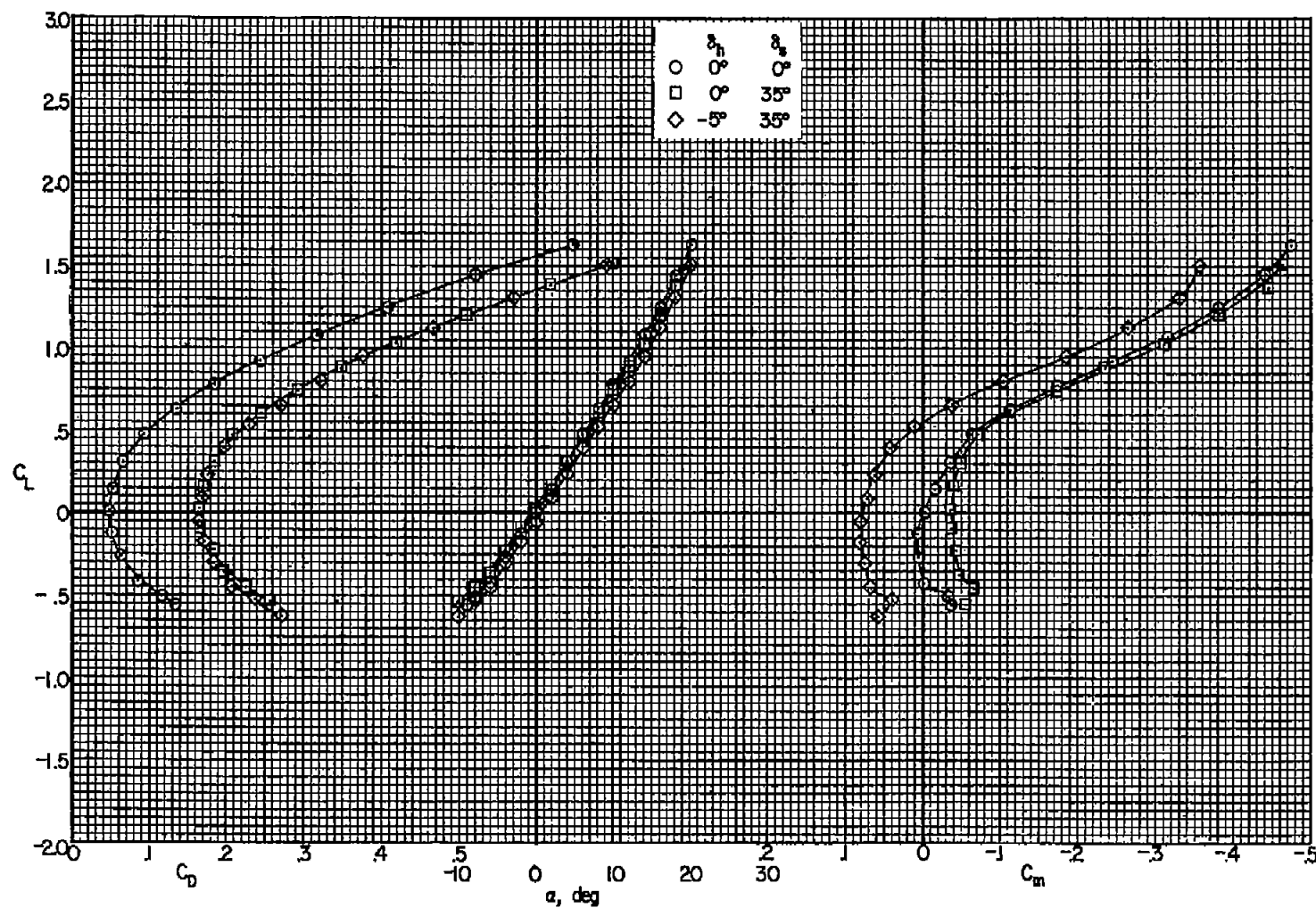


Figure 5.- The effects of speed brakes on the lift, drag, and pitching-moment coefficients; wing, modified body, empennage.



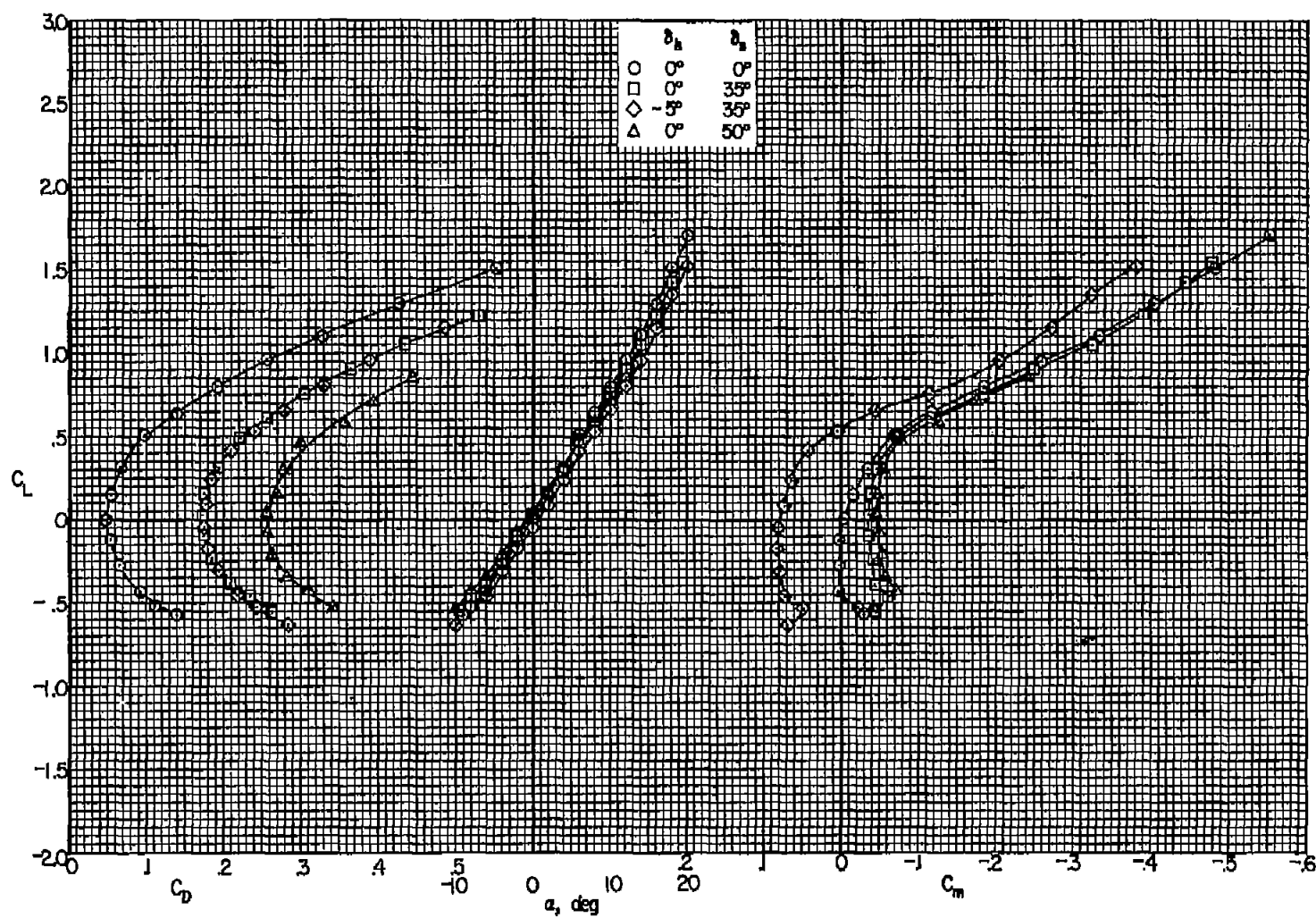
(b) $M = 0.80$

Figure 5.- Continued.



(c) $M = 0.90$

Figure 5.- Continued.



(d) $M = 0.92$

Figure 5.- Concluded.

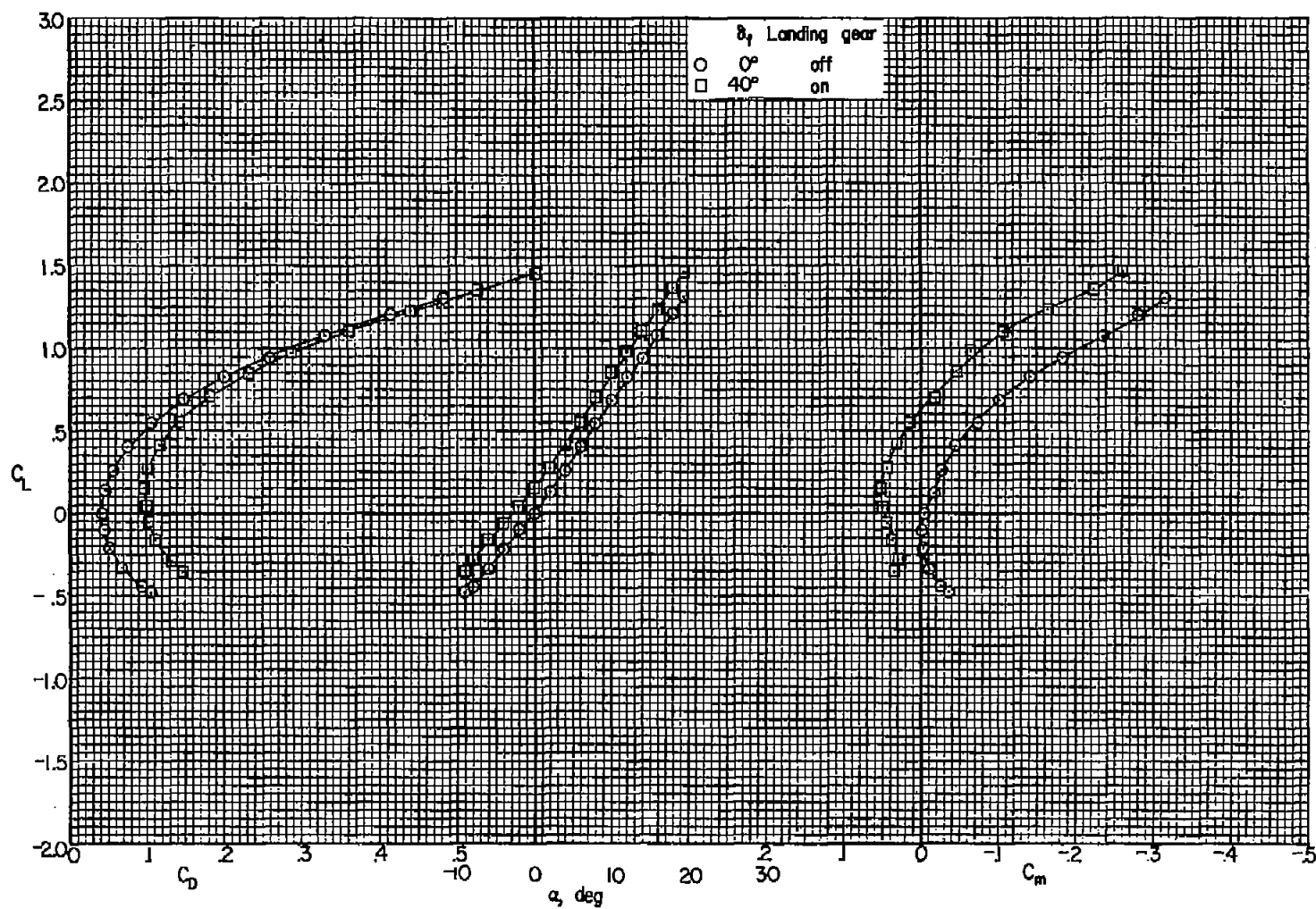


Figure 6.- The effects of flaps and landing gear on the lift, drag, and pitching-moment coefficients; $\delta_h = 0^\circ$, $M = 0.22$.

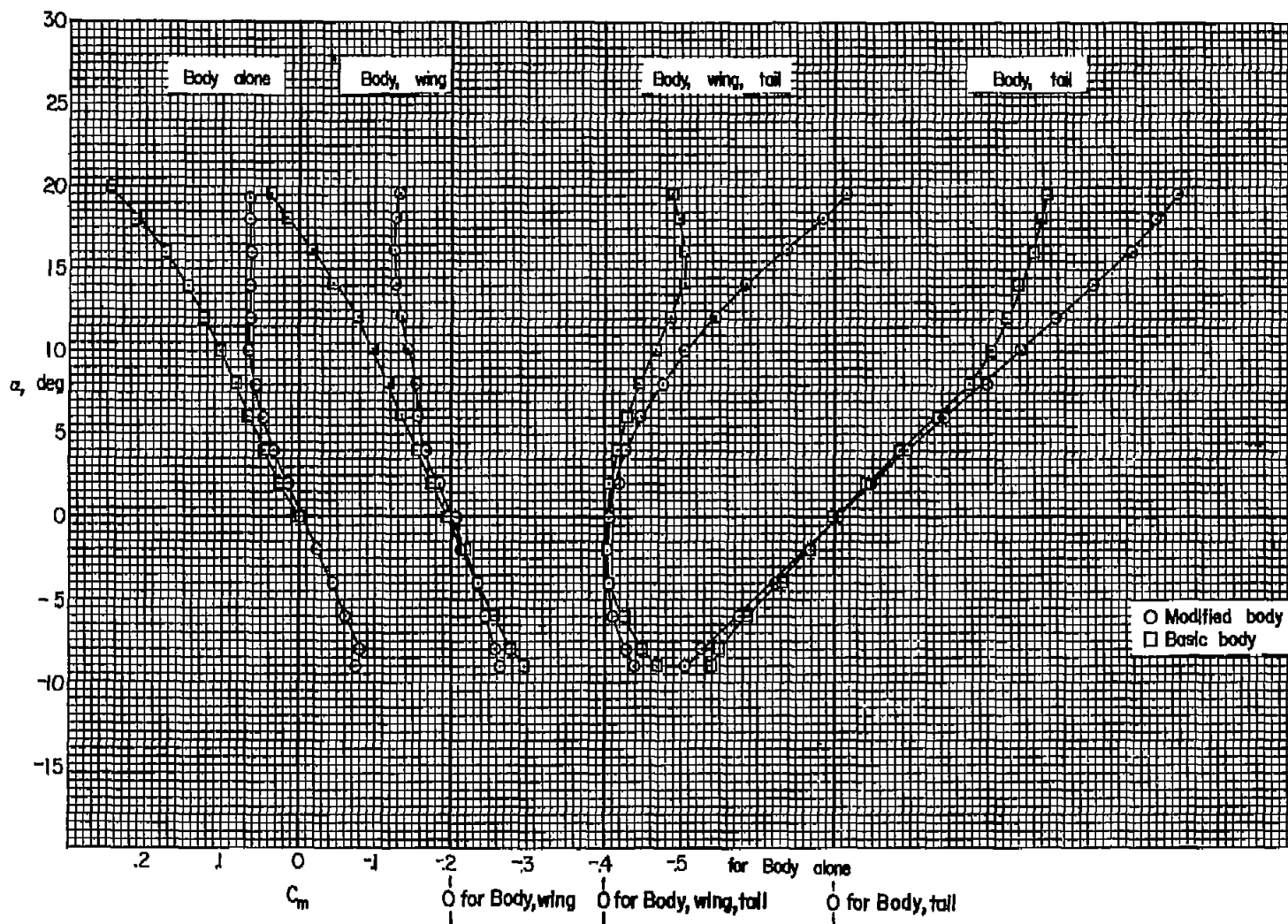


Figure 7.- The effects of body modification on the pitching moment; $M = 0.22$.

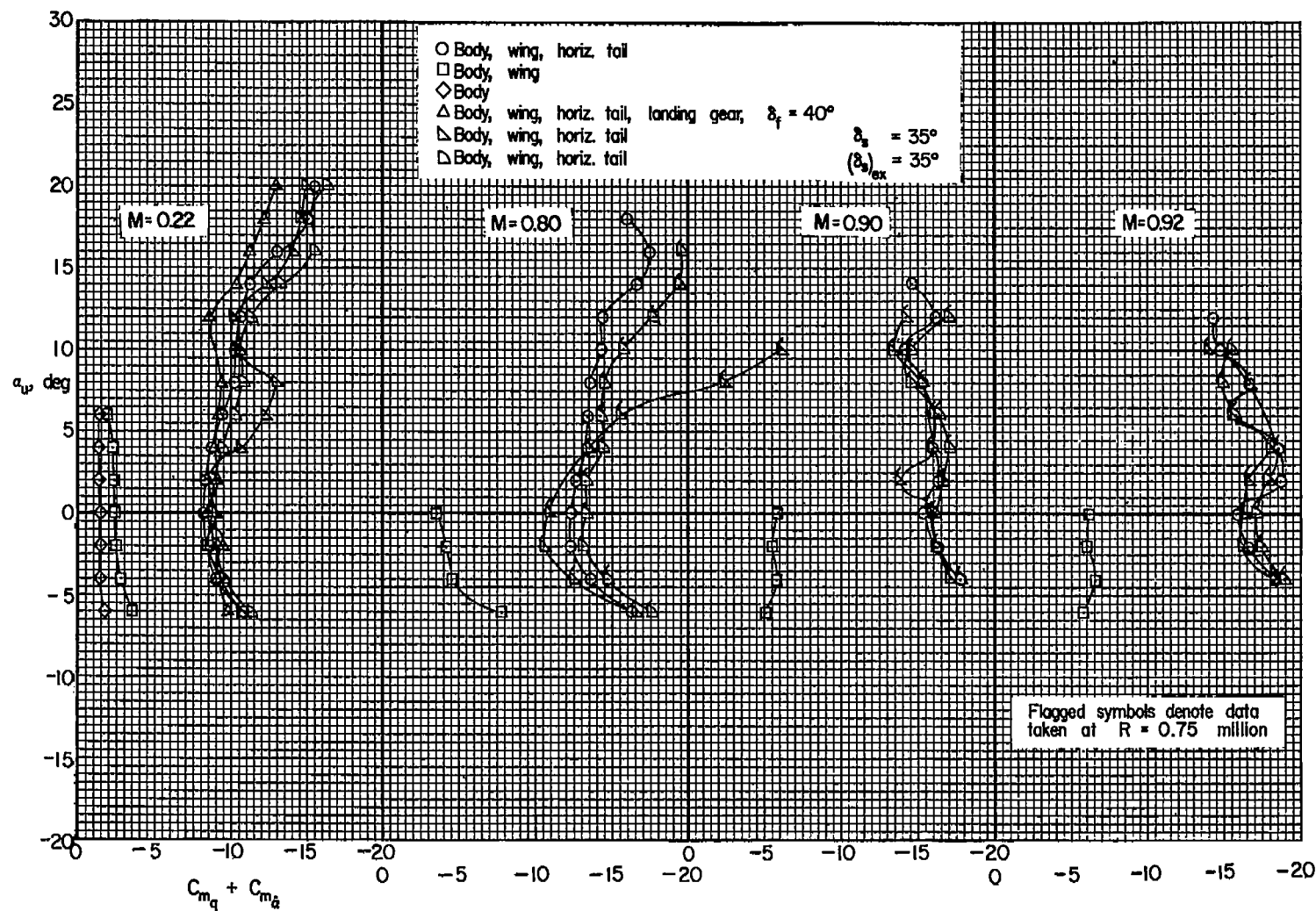


Figure 8.- Damping-in-pitch characteristics; original body and vertical tails.

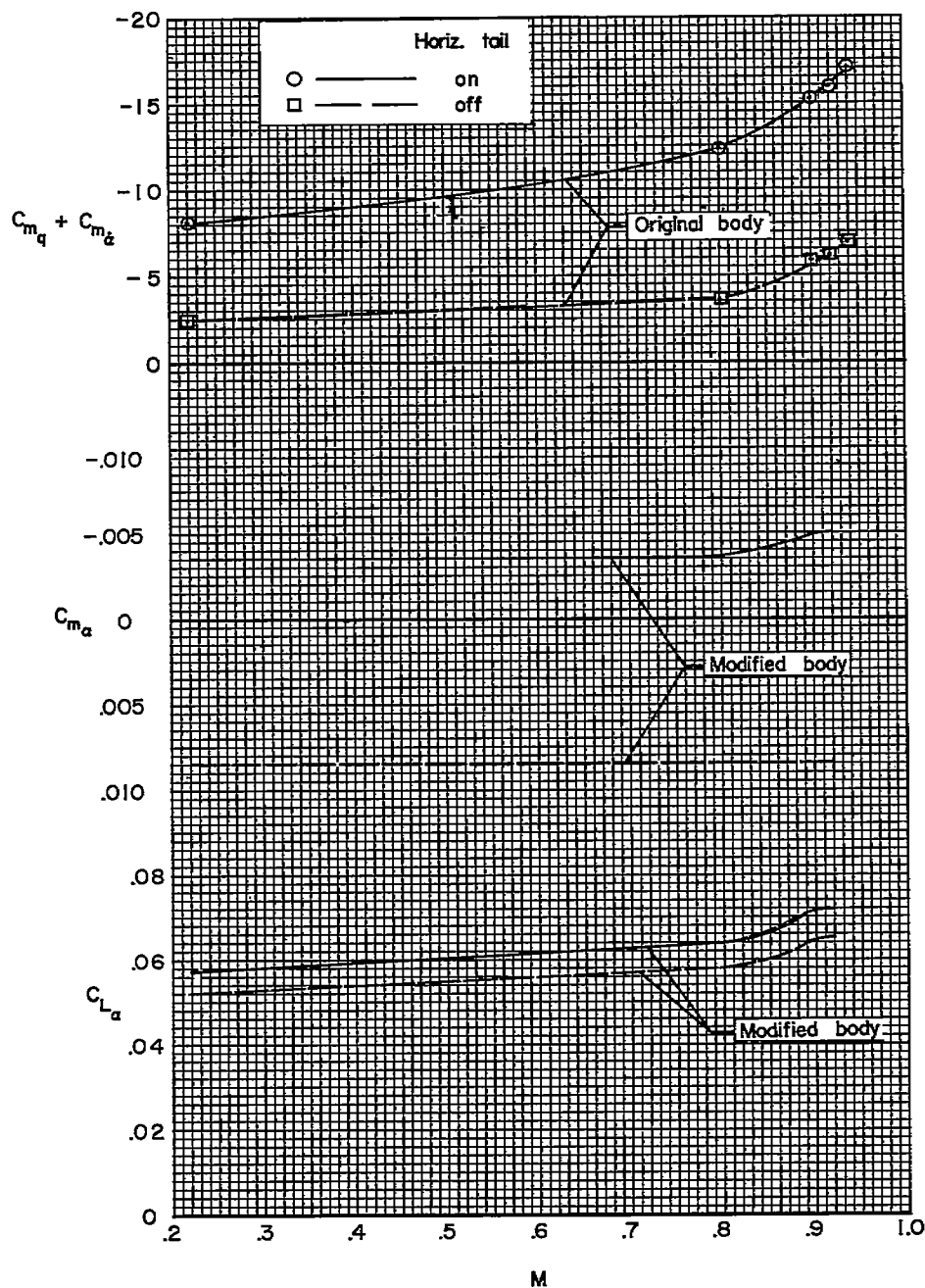


Figure 9.- Variation with Mach number of the longitudinal static and dynamic stability derivatives; $\alpha = 0^\circ$.

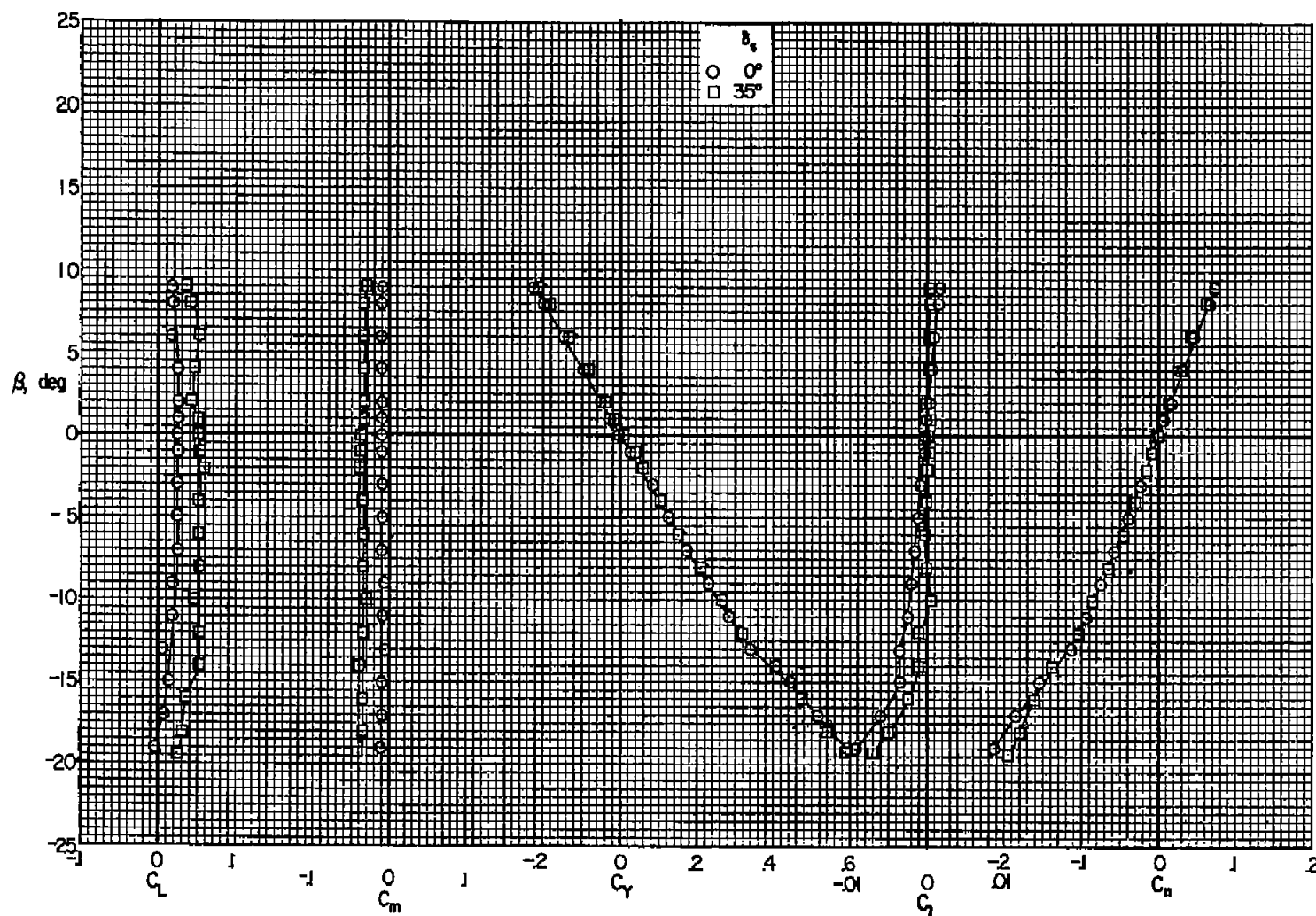
(a) $M = 0.22$

Figure 10.- The variation with sideslip angle of the static forces and moments; wing, modified body, horizontal tail, upper vertical tail, and large lower vertical tail; $\alpha = 0^\circ$.

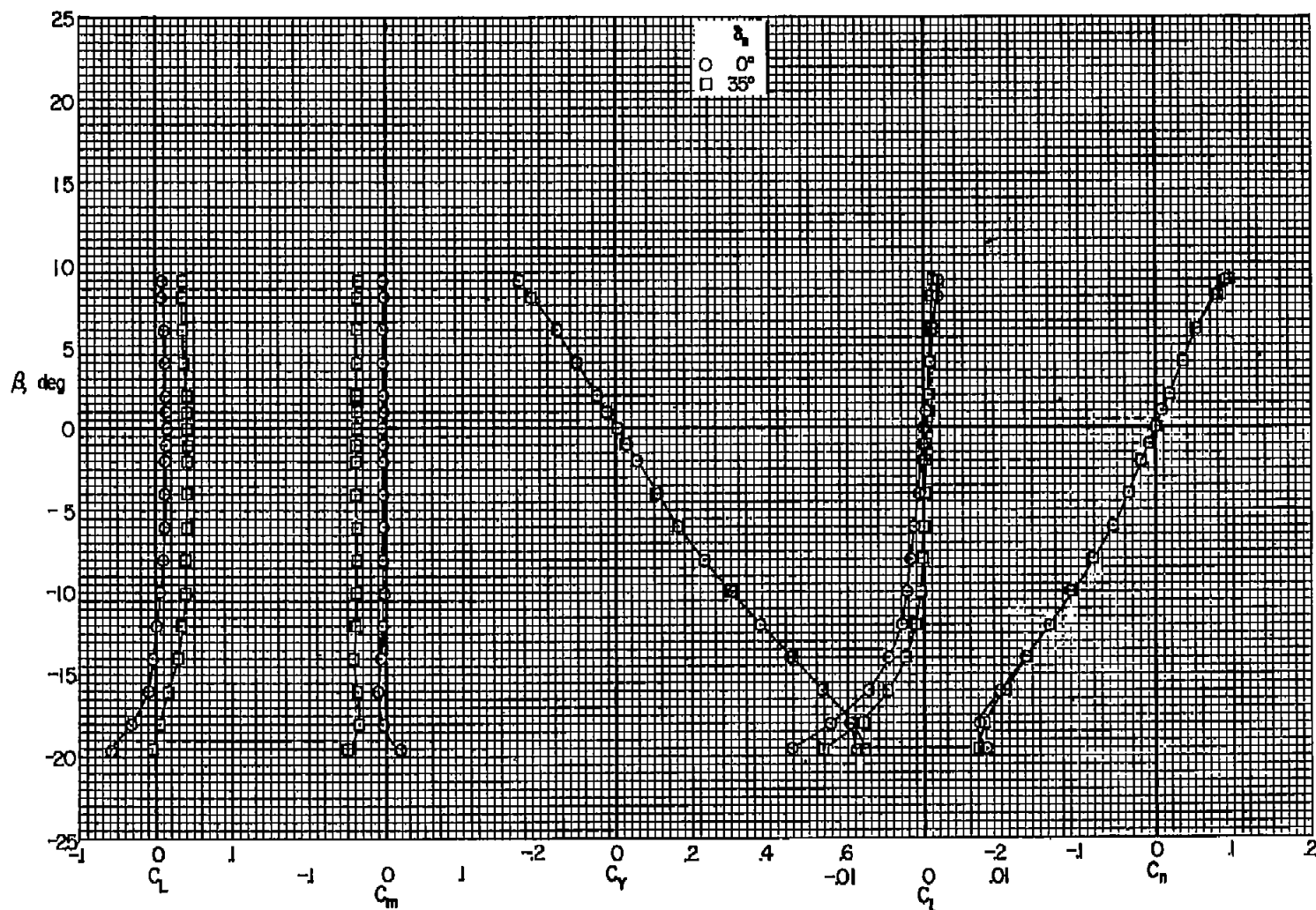
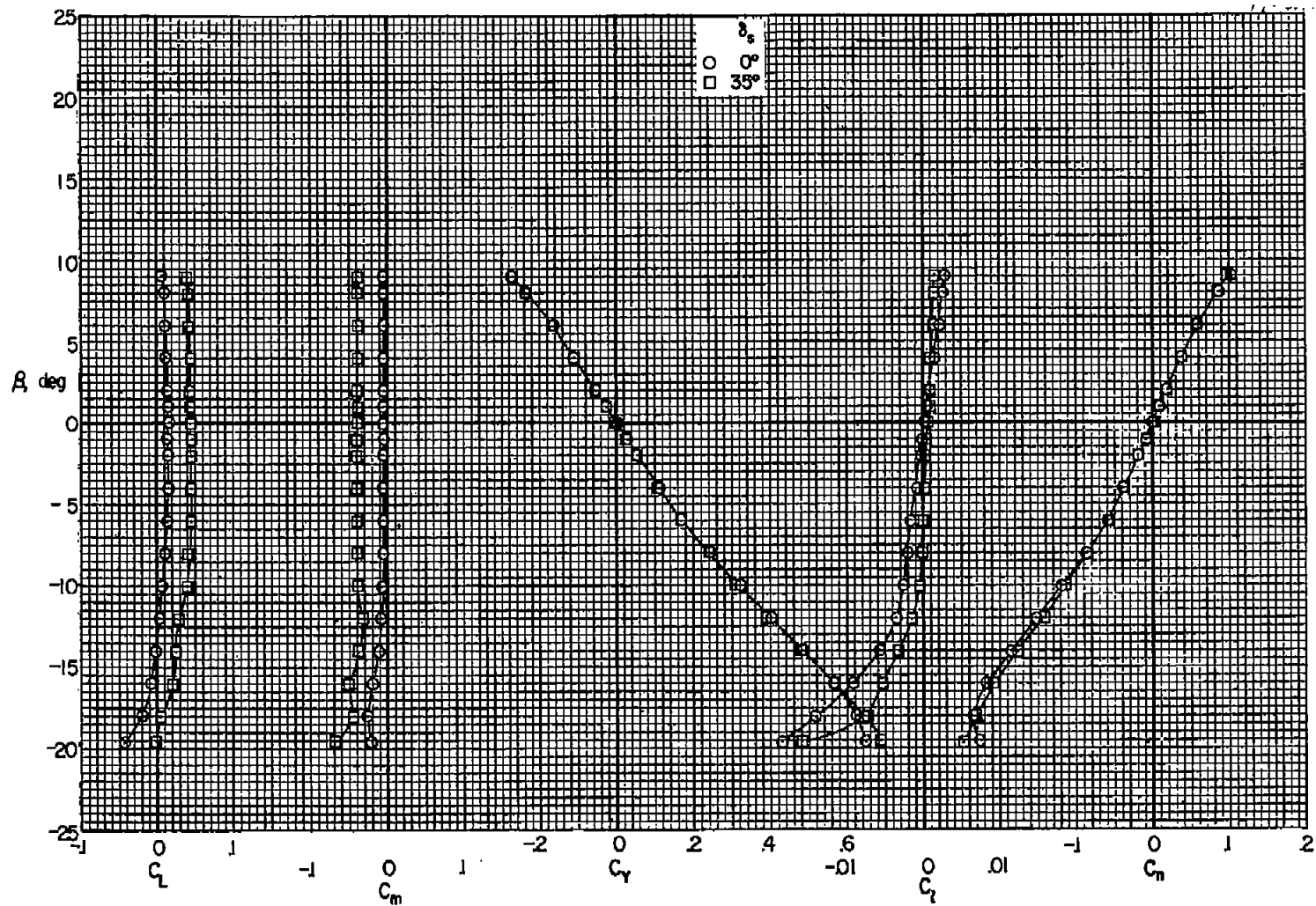
(b) $M = 0.80$

Figure 10.- Continued.



(c) $M = 0.90$

Figure 10.- Continued.

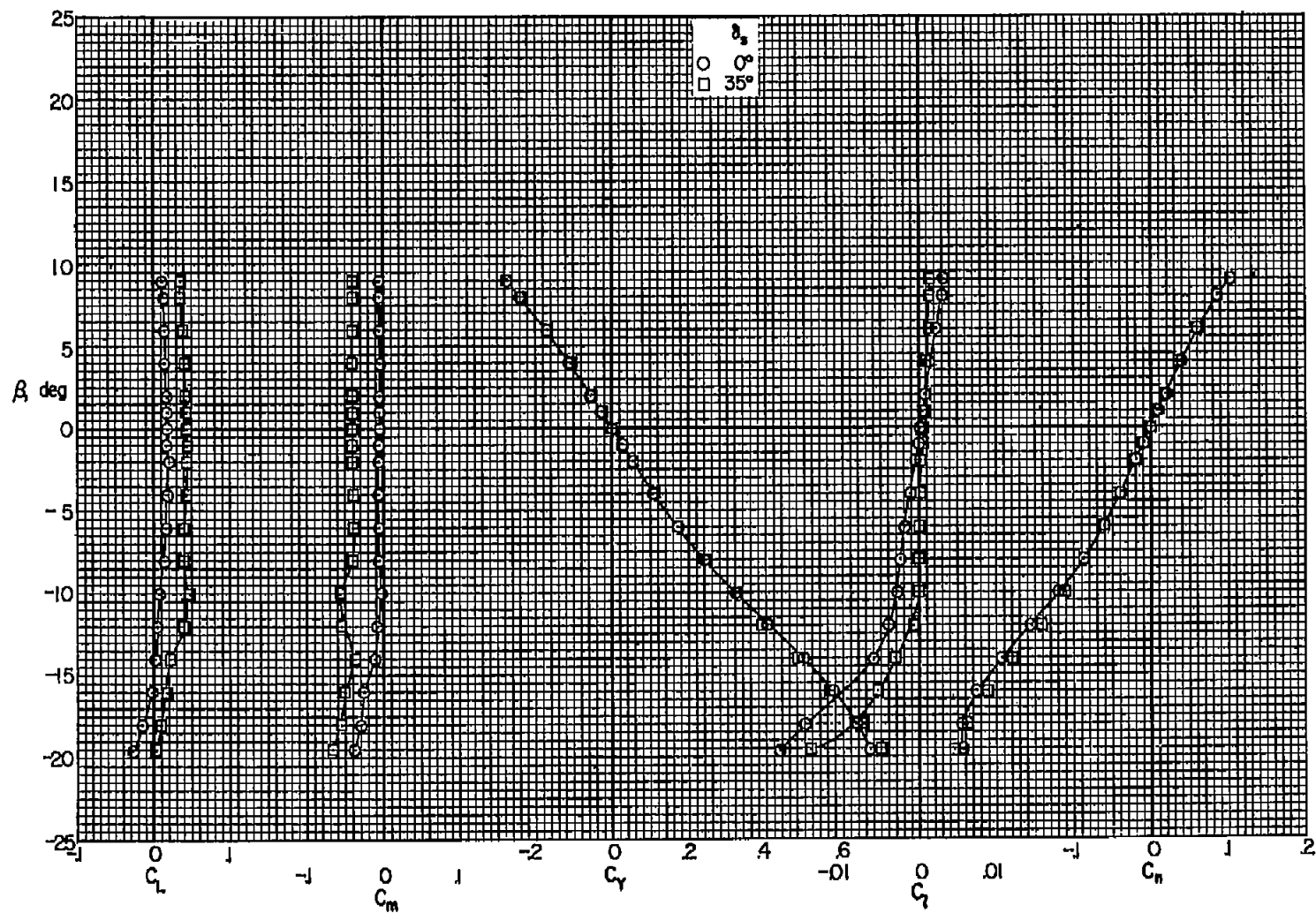
(d) $M = 0.92$

Figure 10.- Concluded.

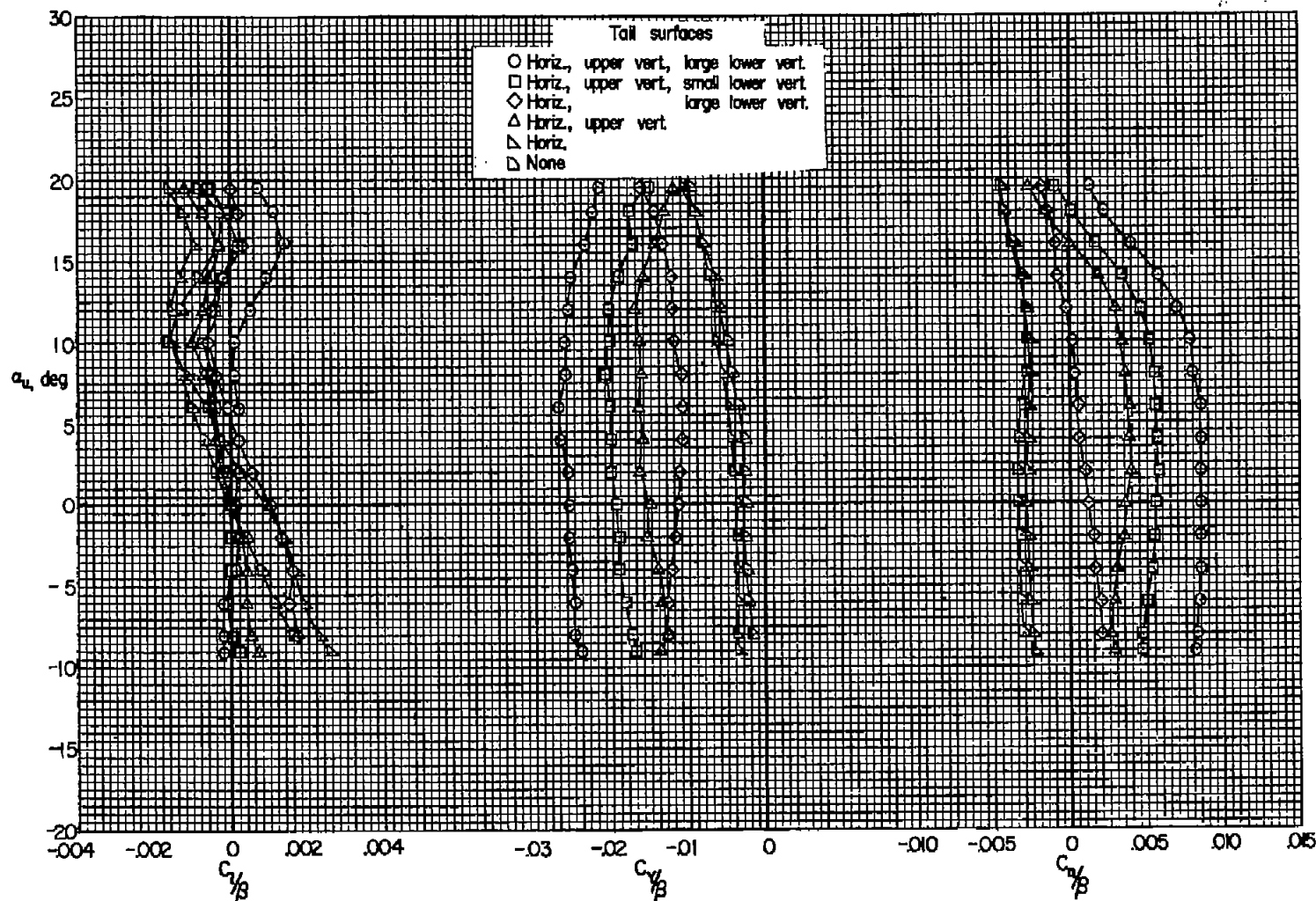
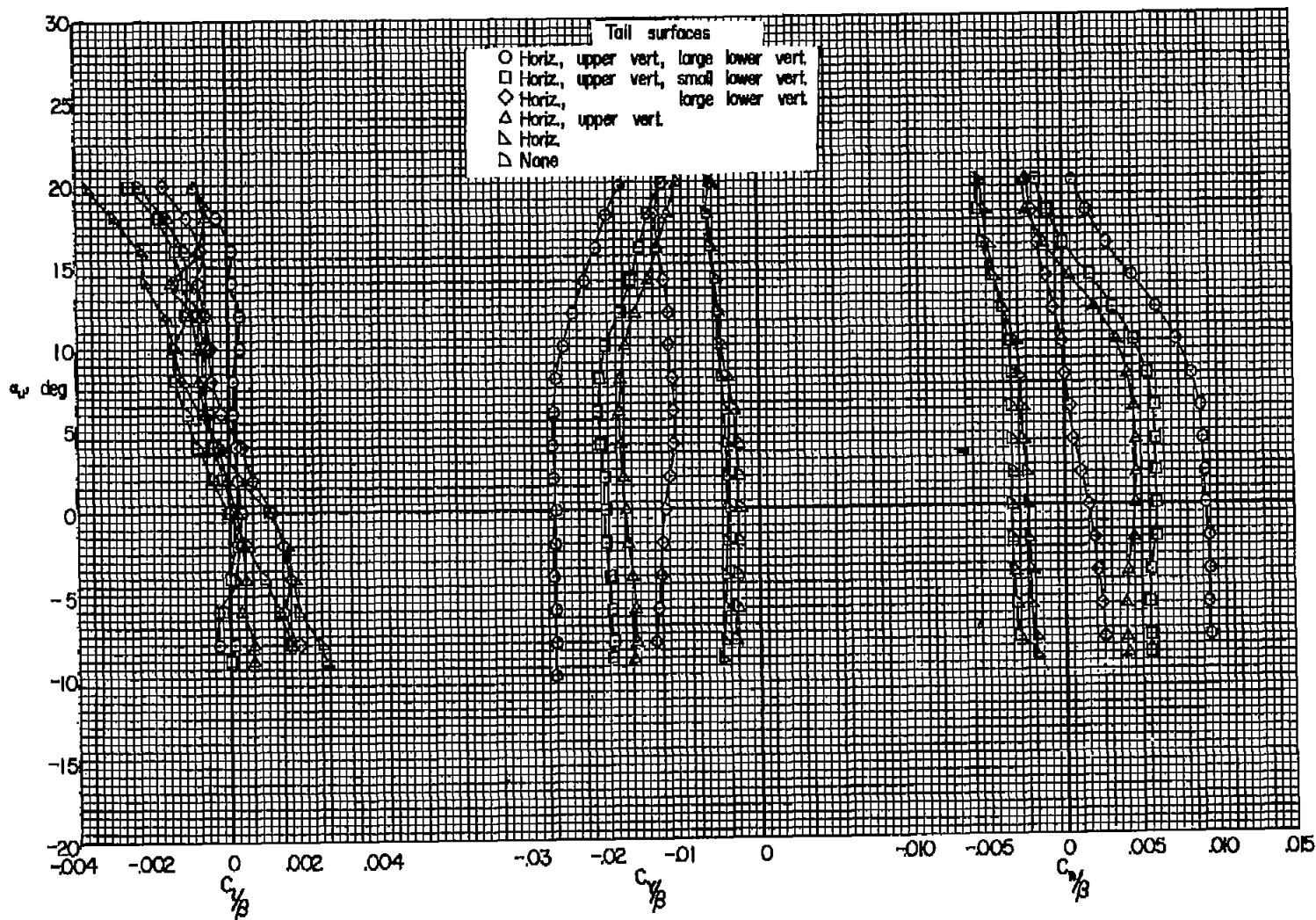
(a) $M = 0.22$

Figure 11.- The variation with angle of attack of the lateral-directional static-stability derivatives of the model with several empennage configurations; wing and modified body.



(b) $M = 0.80$

Figure 11.- Continued.

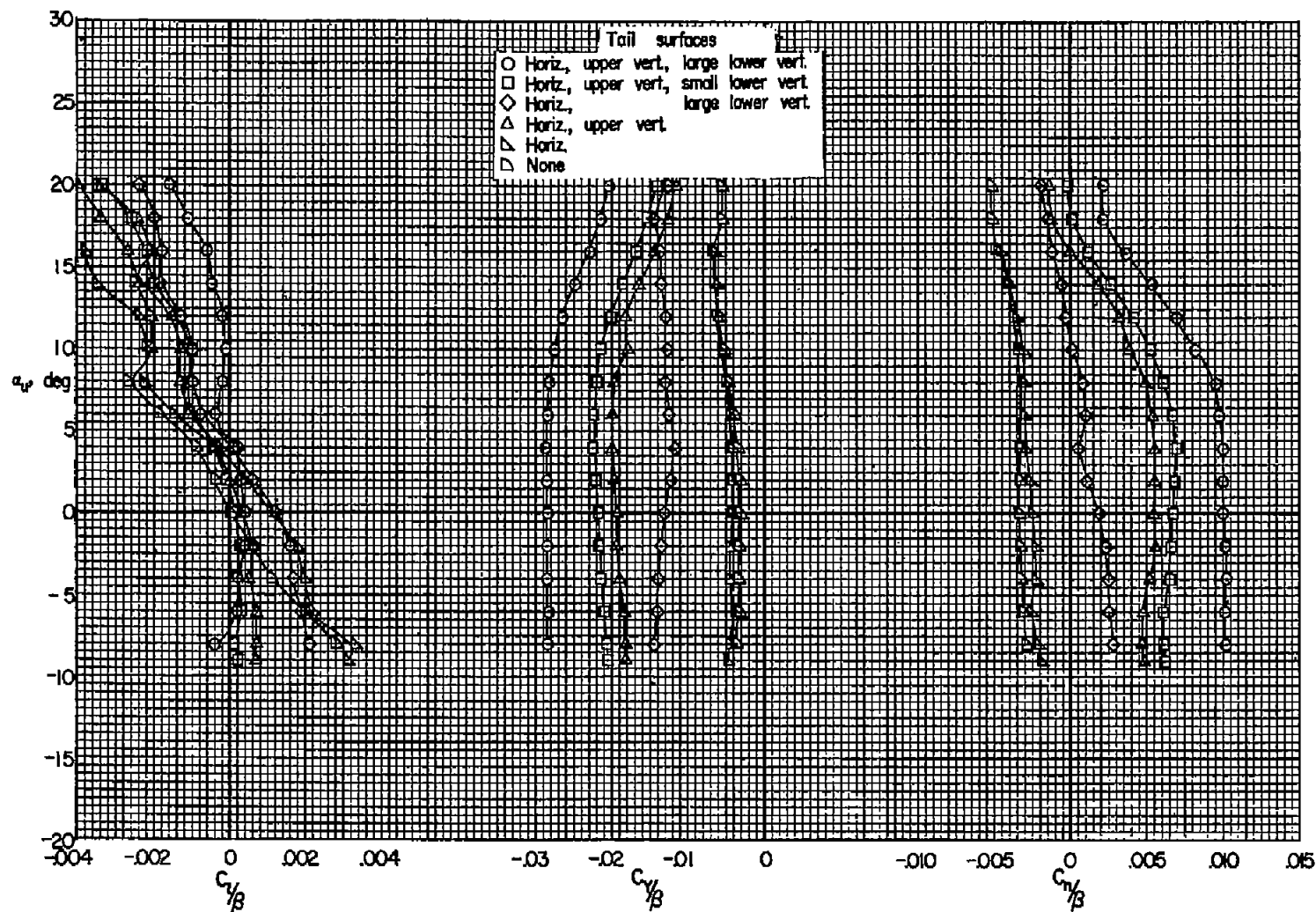
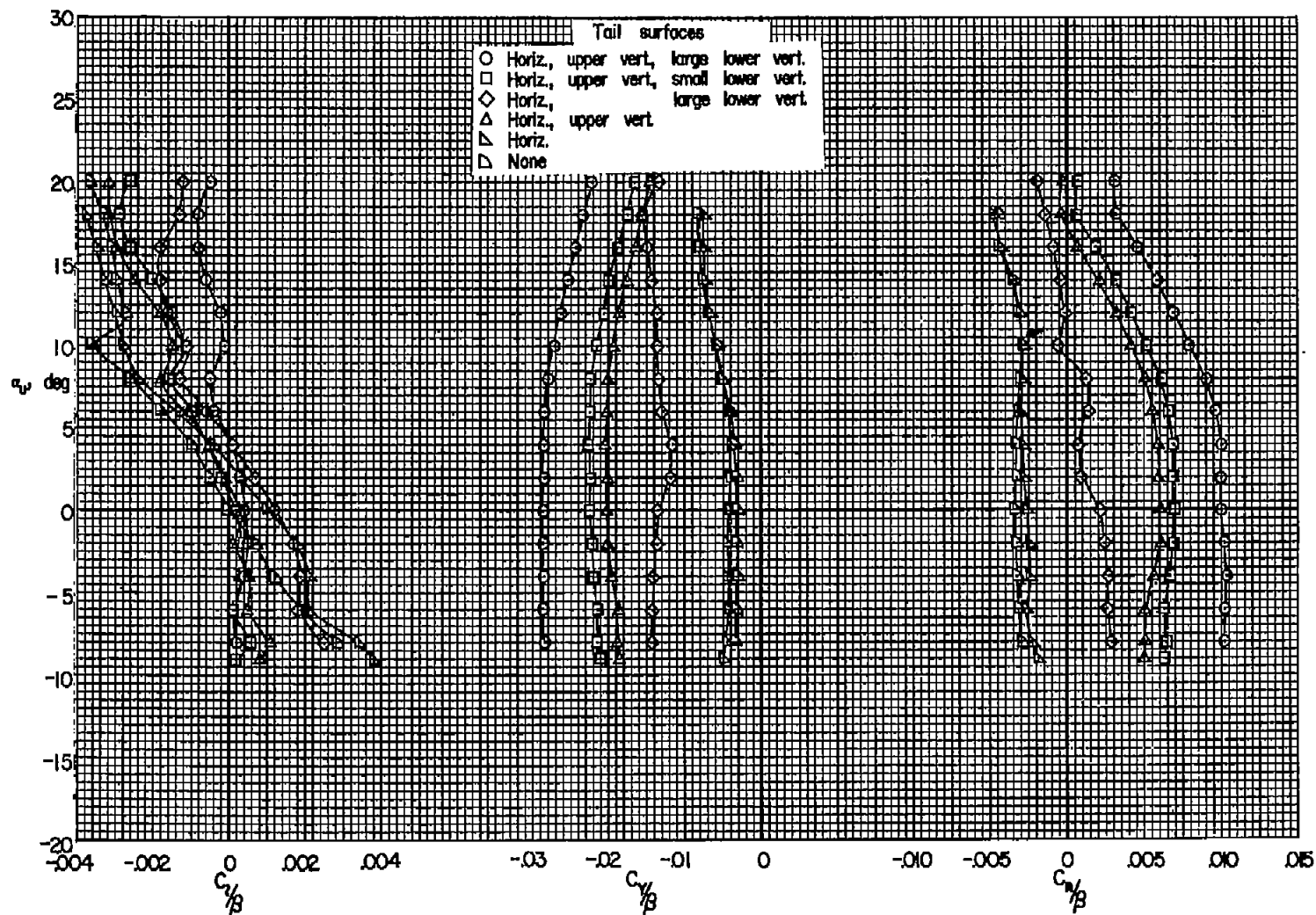
(c) $M = 0.90$

Figure 11.- Continued.



(d) $M = 0.92$

Figure 11.- Concluded.

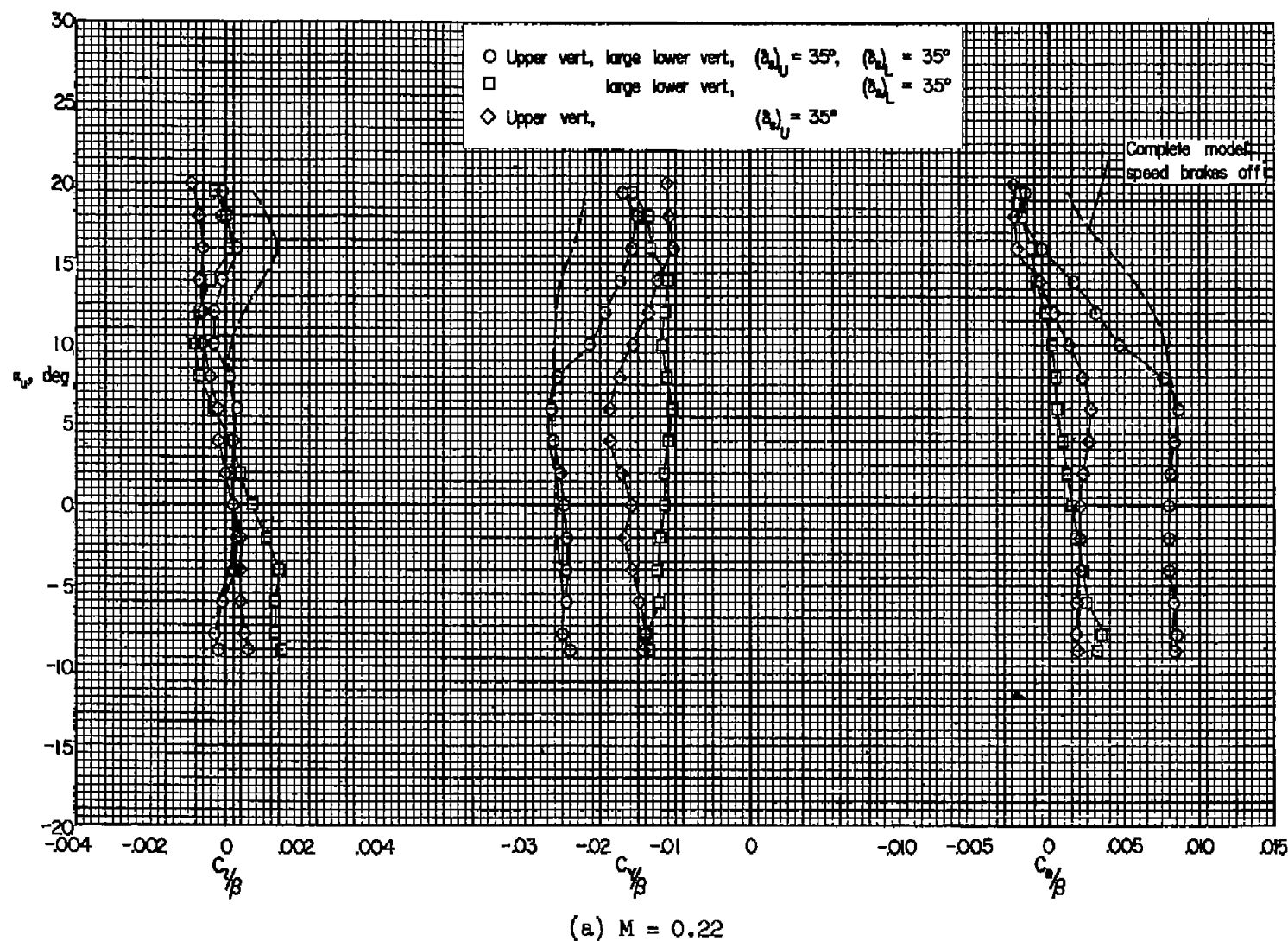
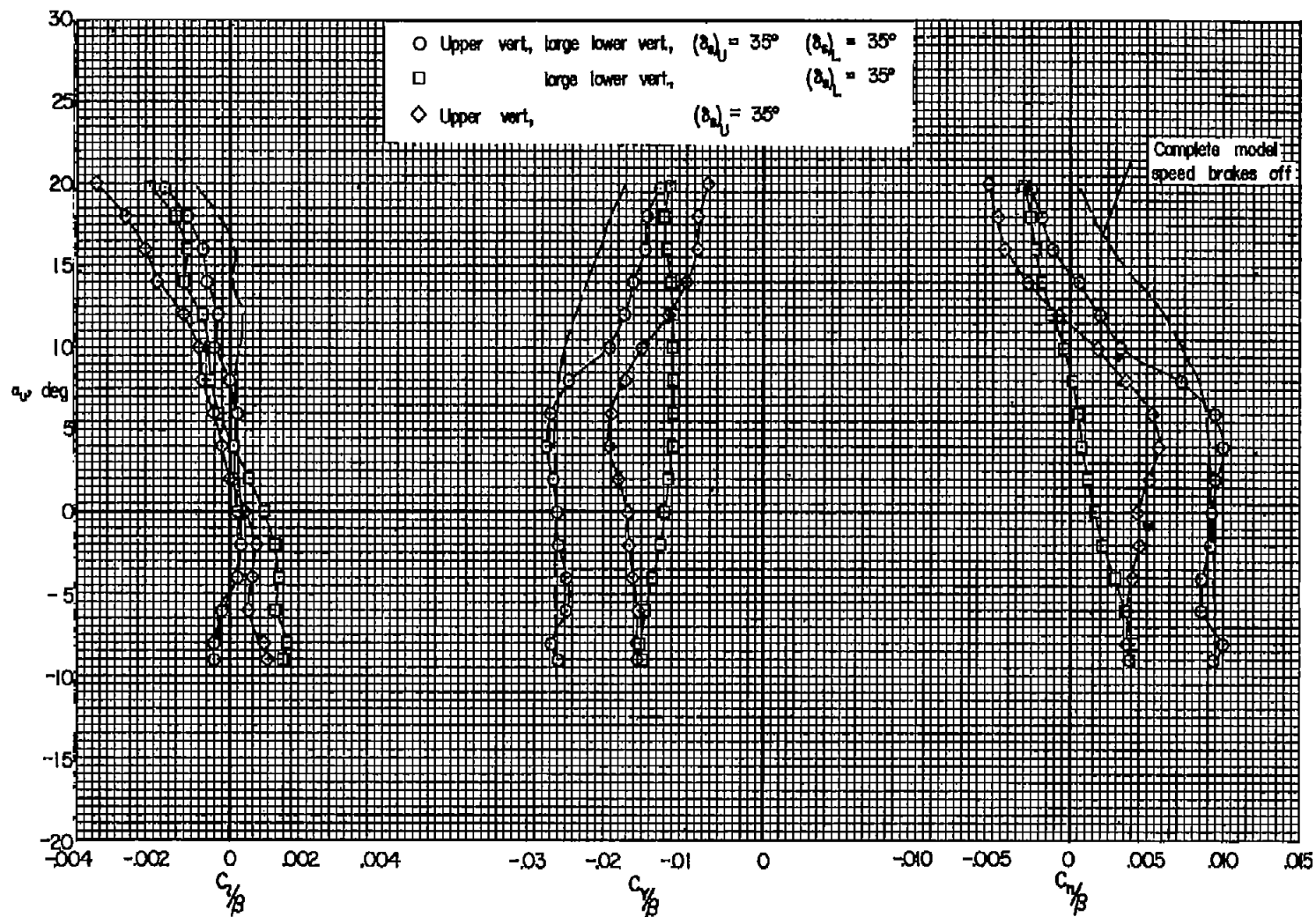
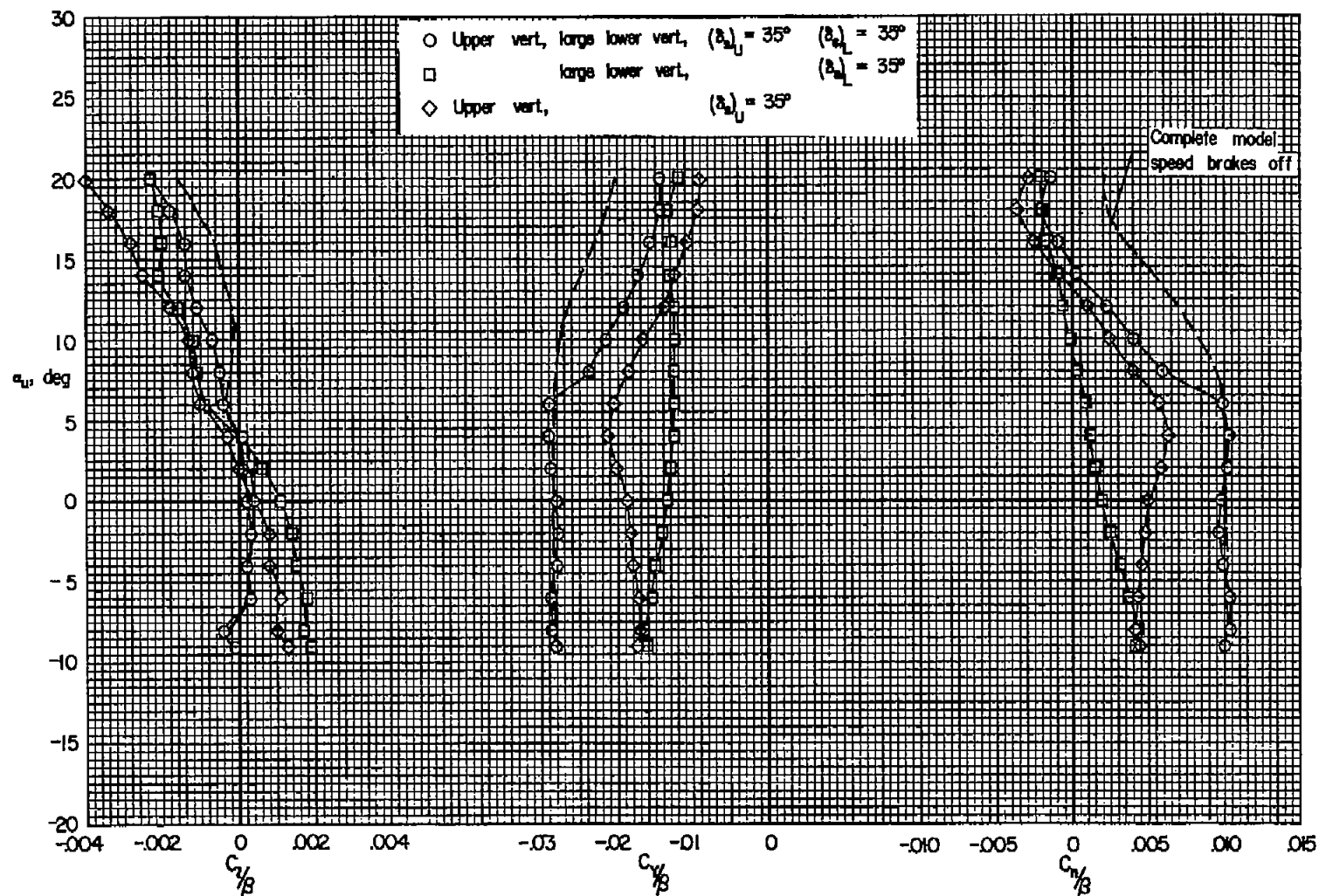


Figure 12.- Effects of individual speed-brake deflection on the lateral-directional static stability derivatives; wing, modified body, and horizontal tail.



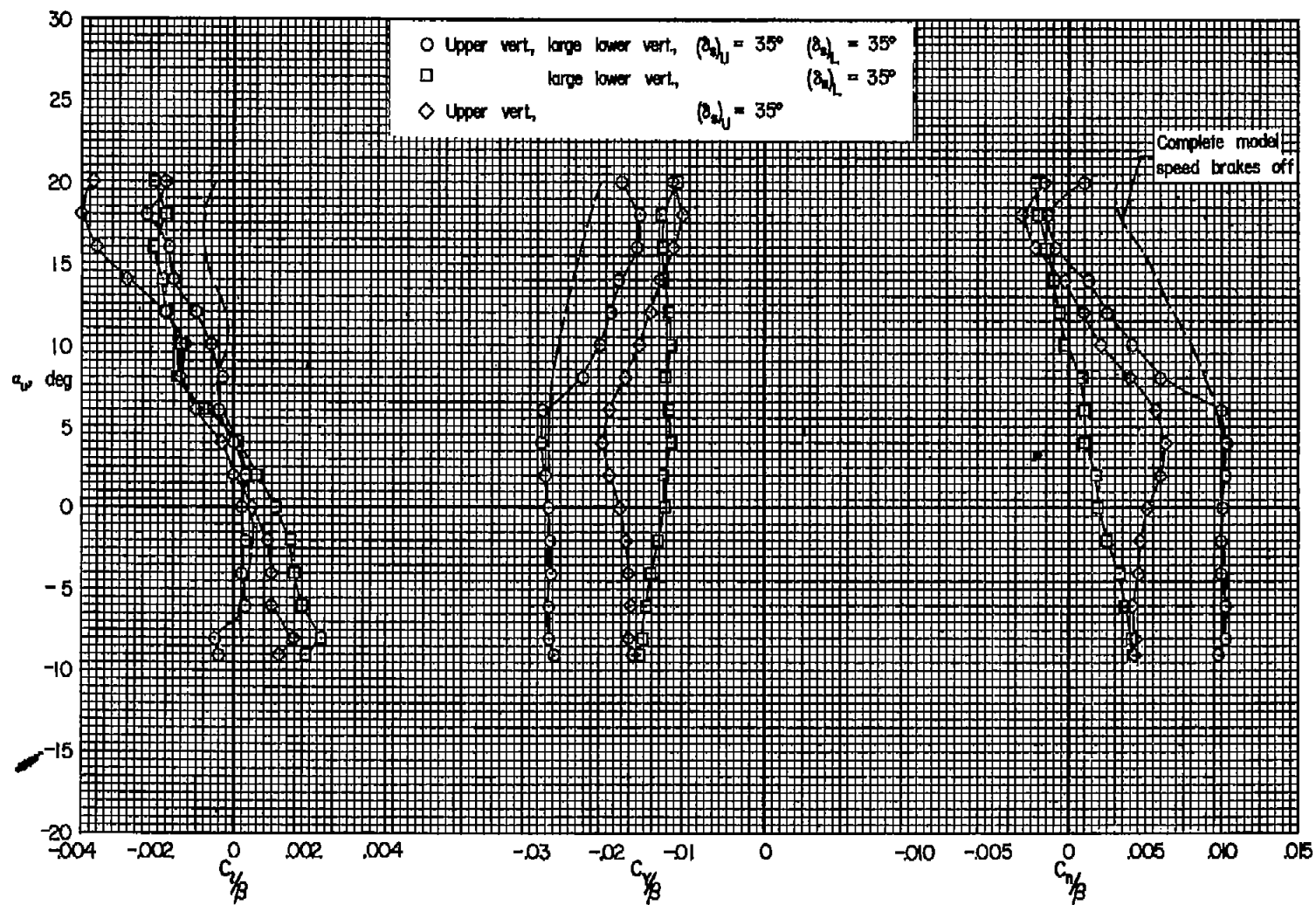
(b) $M = 0.80$

Figure 12.- Continued.



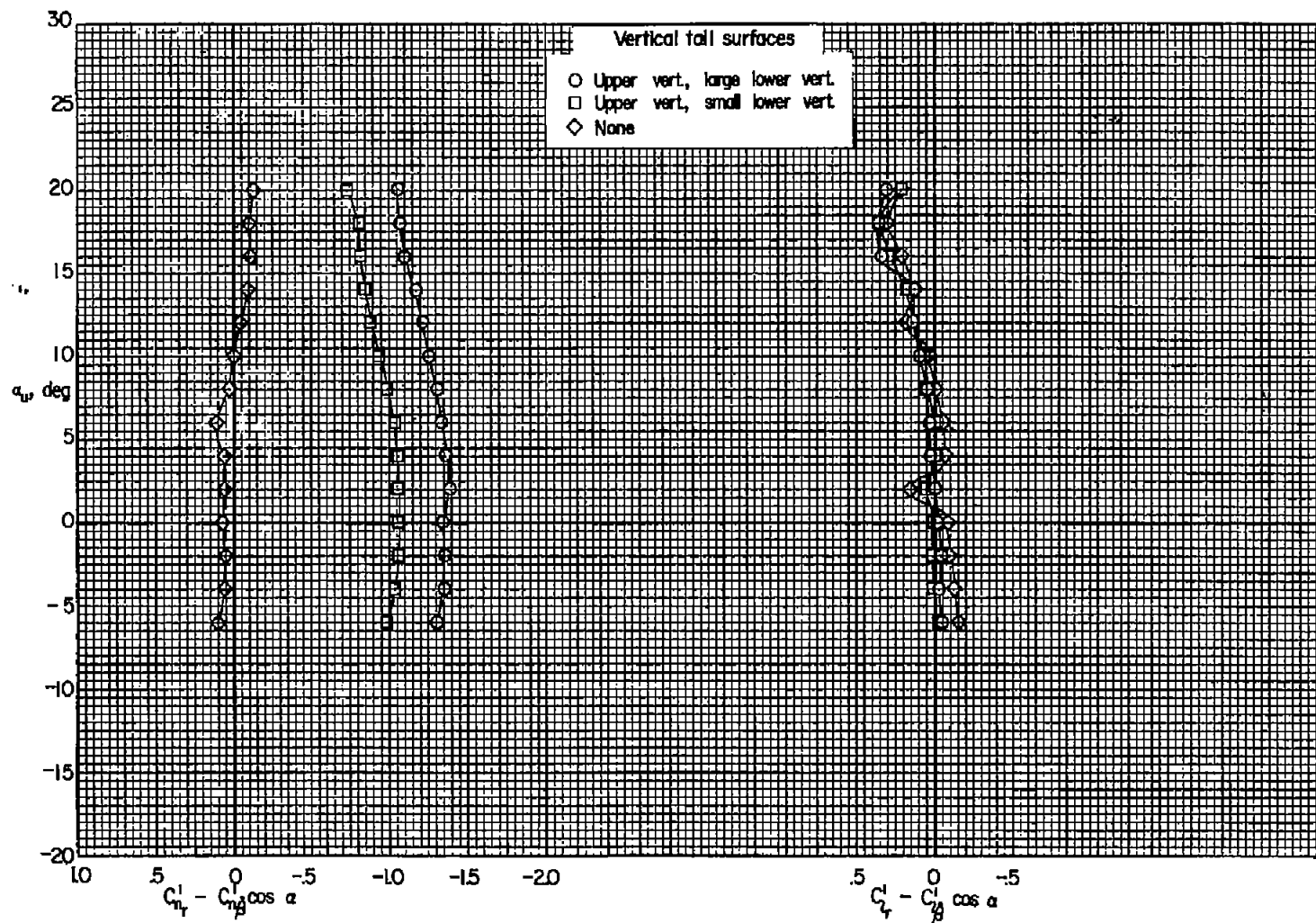
(c) $M = 0.90$

Figure 12.- Continued.



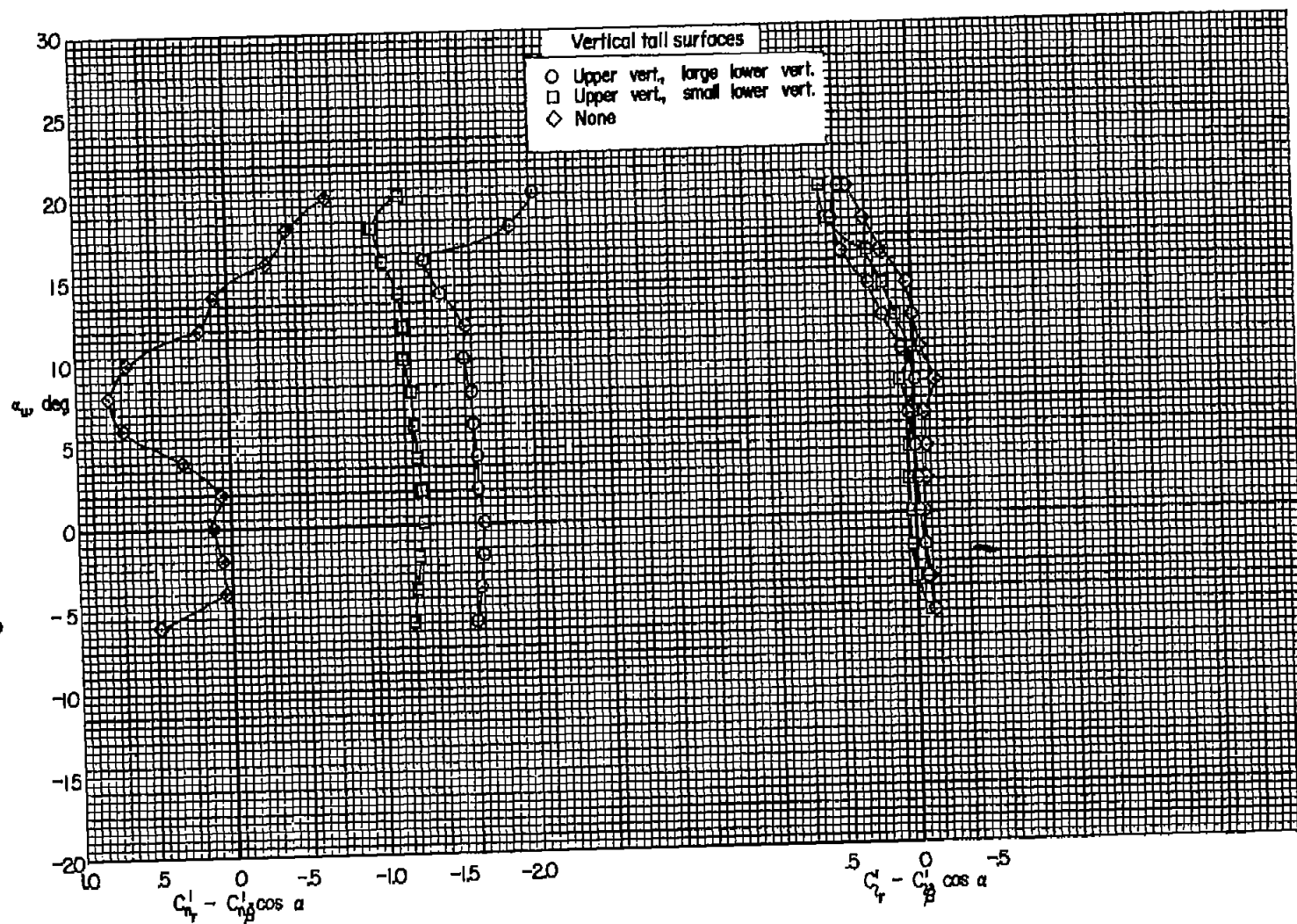
(d) $M = 0.92$

Figure 12.- Concluded.



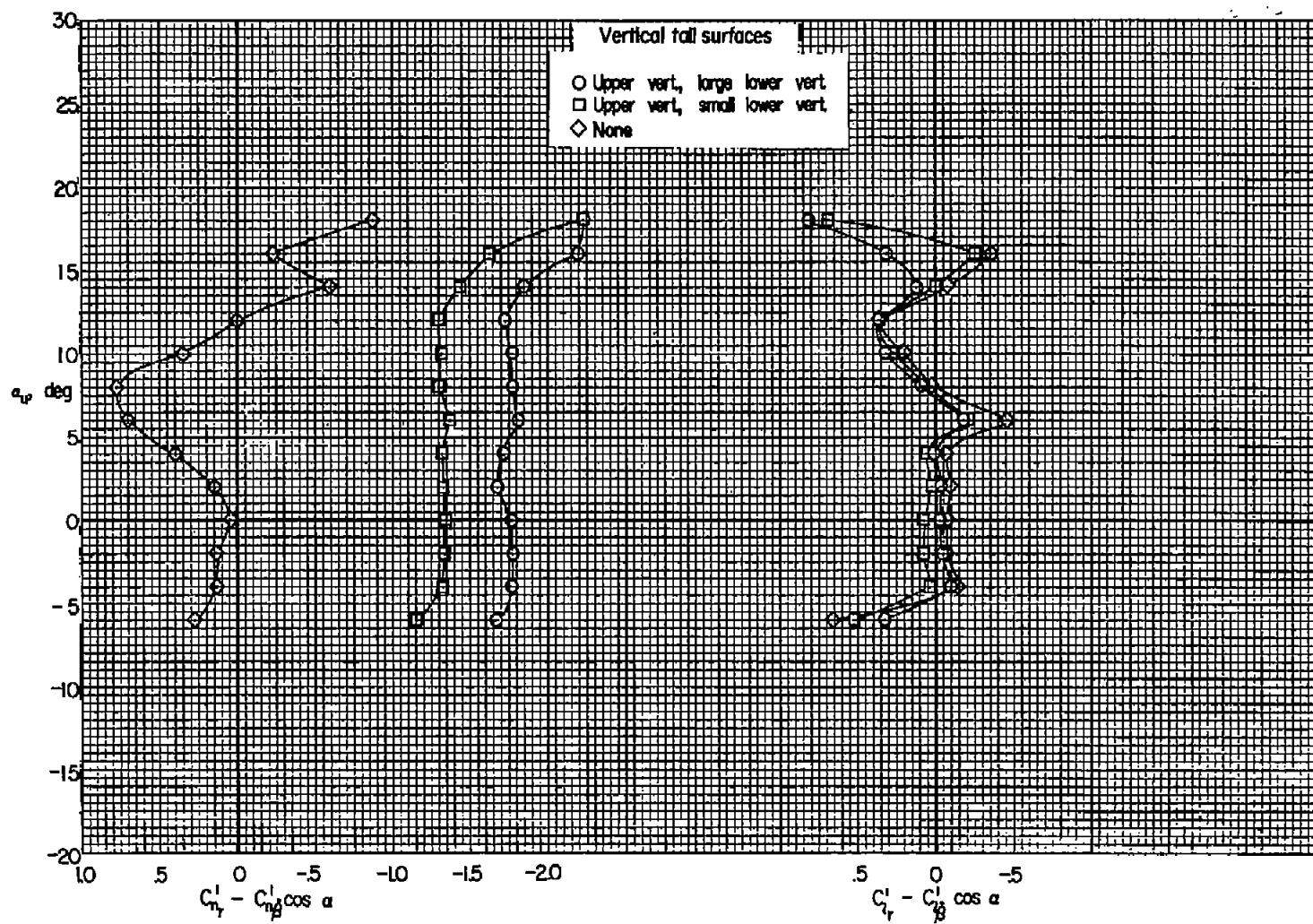
(a) $M = 0.22$

Figure 13.- Damping in yaw and rolling moment due to yawing velocity coefficients; wing, original body, and horizontal tail.



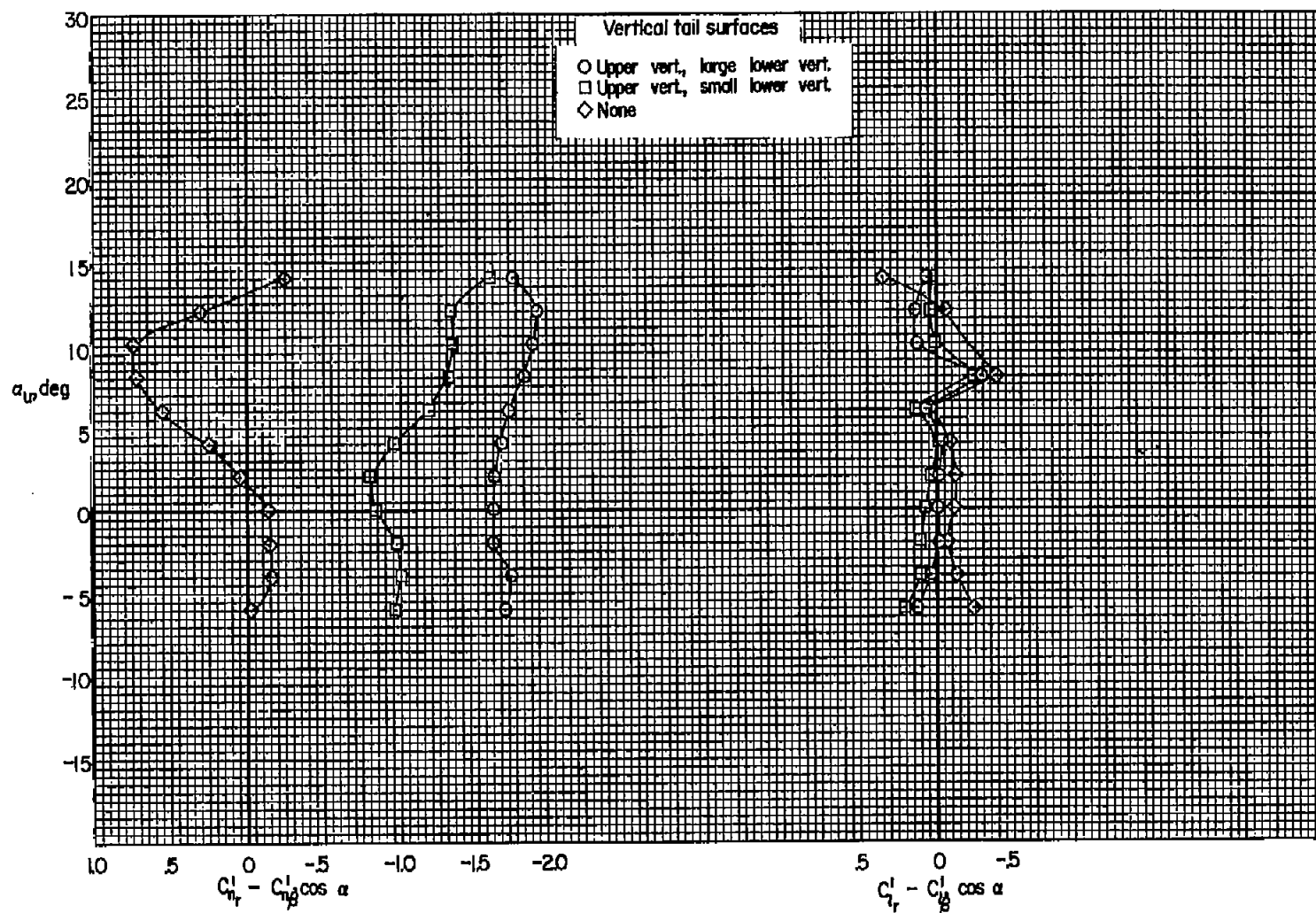
(b) M = 0.80

Figure 13.- Continued.



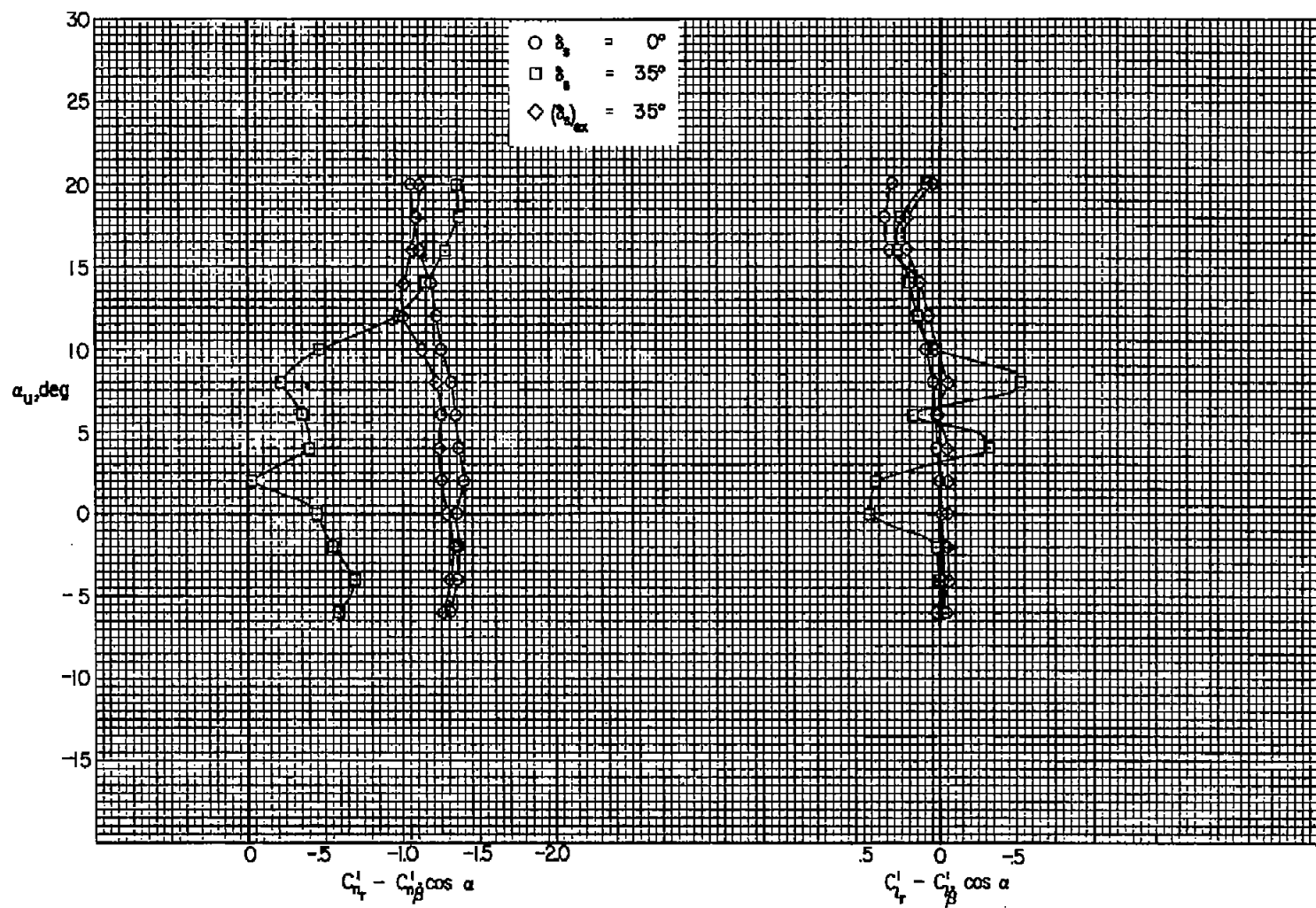
(c) $M = 0.90$

Figure 13.- Continued.



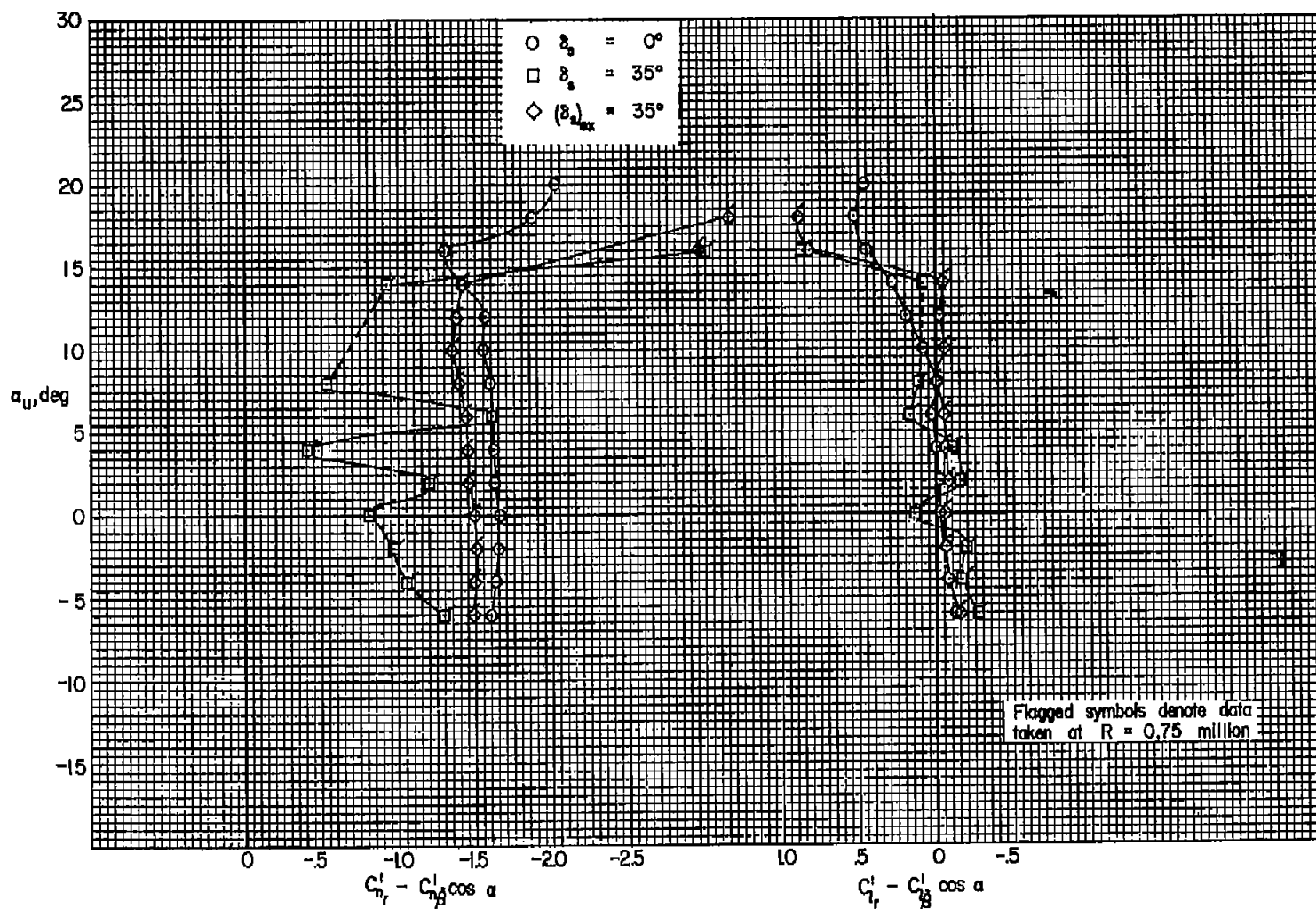
(d) $M = 0.94$

Figure 13.- Concluded.



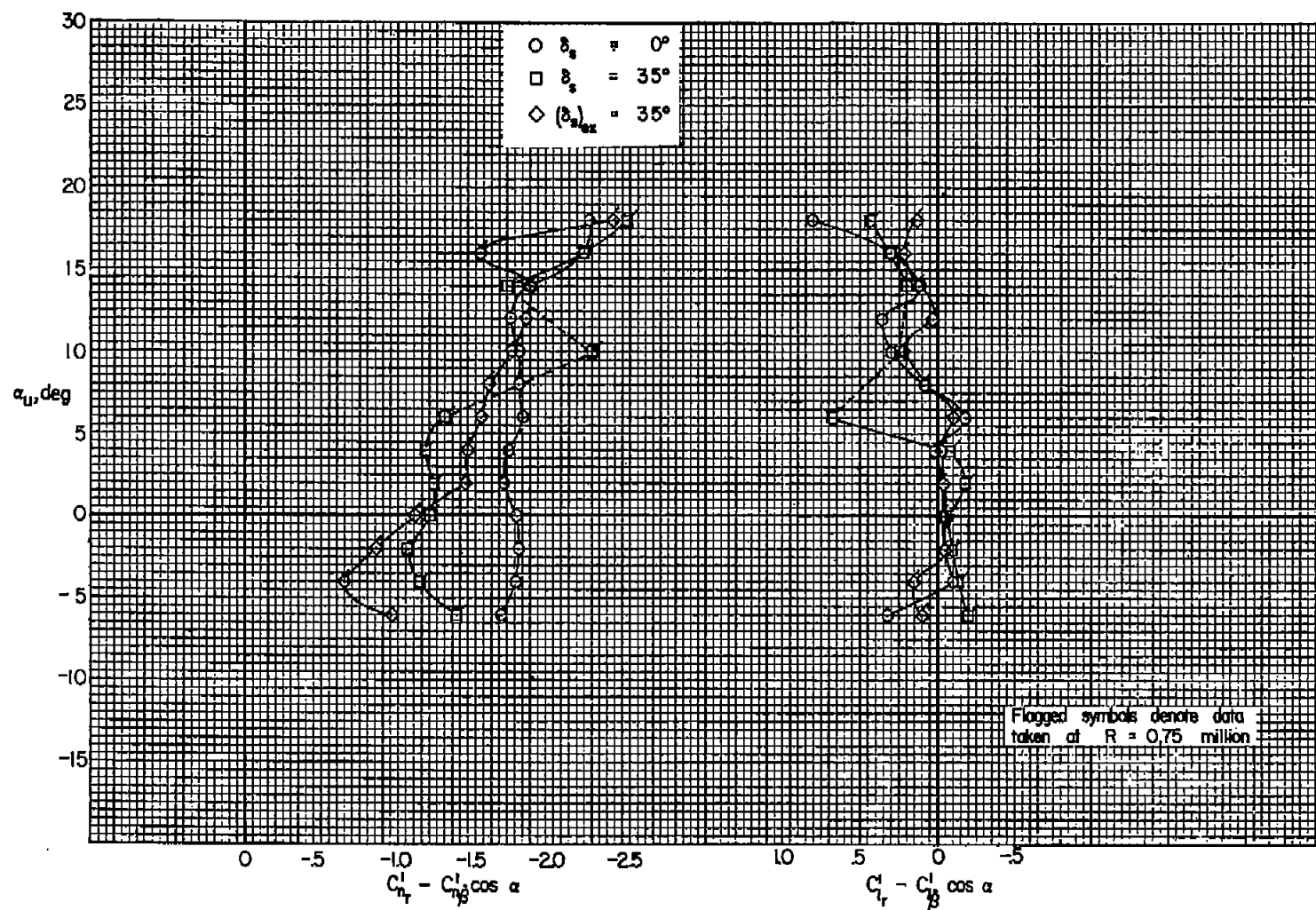
(a) $M = 0.22$

Figure 14.- Effects of speed brakes on the yawing derivatives; wing, original body, horizontal tail, upper vertical tail, and large lower vertical tail.



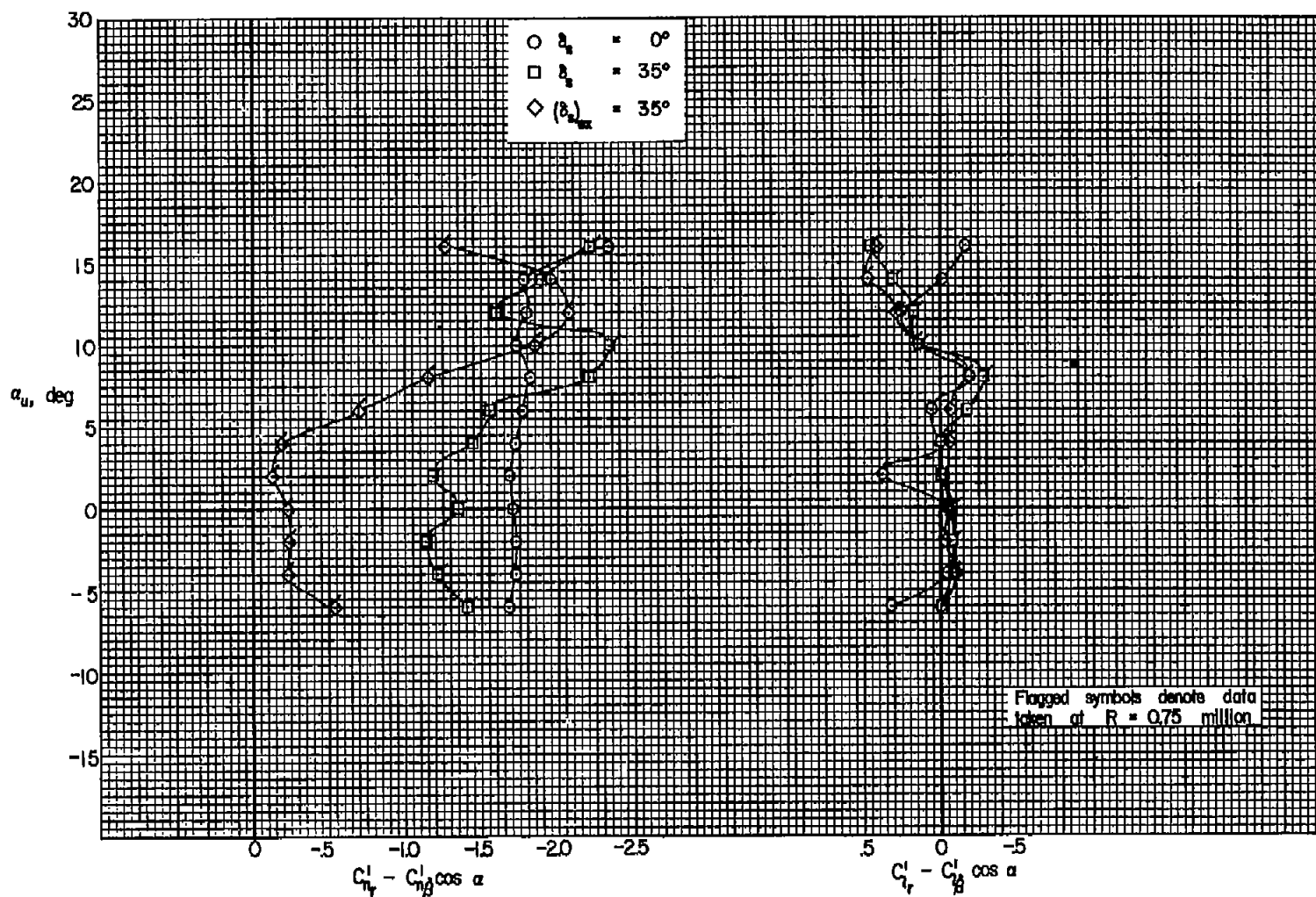
(b) $M = 0.80$

Figure 14.- Continued.



(c) $M = 0.90$

Figure 14.- Continued.



(d) $M = 0.92$

Figure 14.- Concluded.

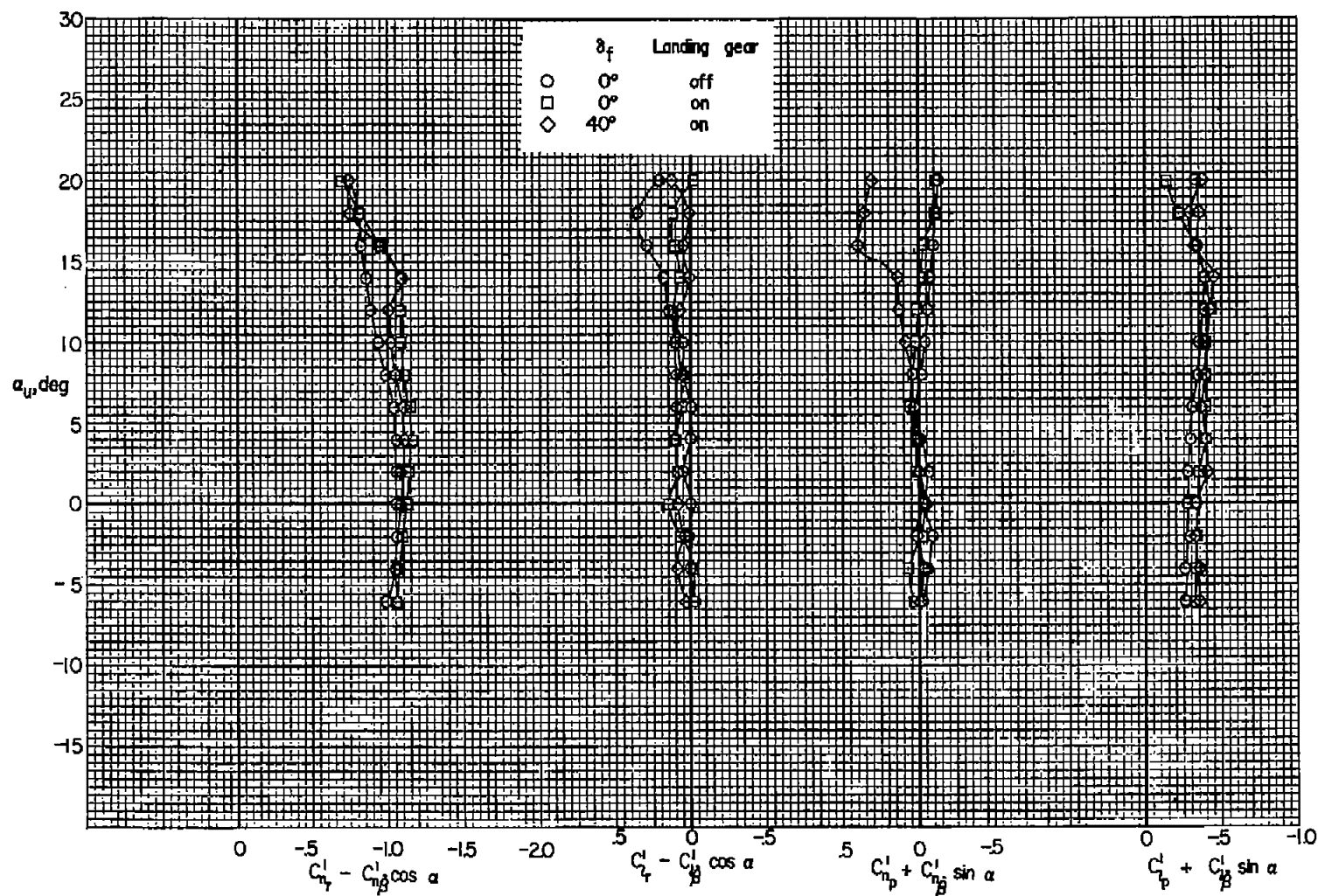


Figure 15.- Effects of landing gear and flaps on the lateral-directional rotary stability derivatives; wing, original body, horizontal tail, upper vertical tail, and small lower vertical tail; $M = 0.22$.

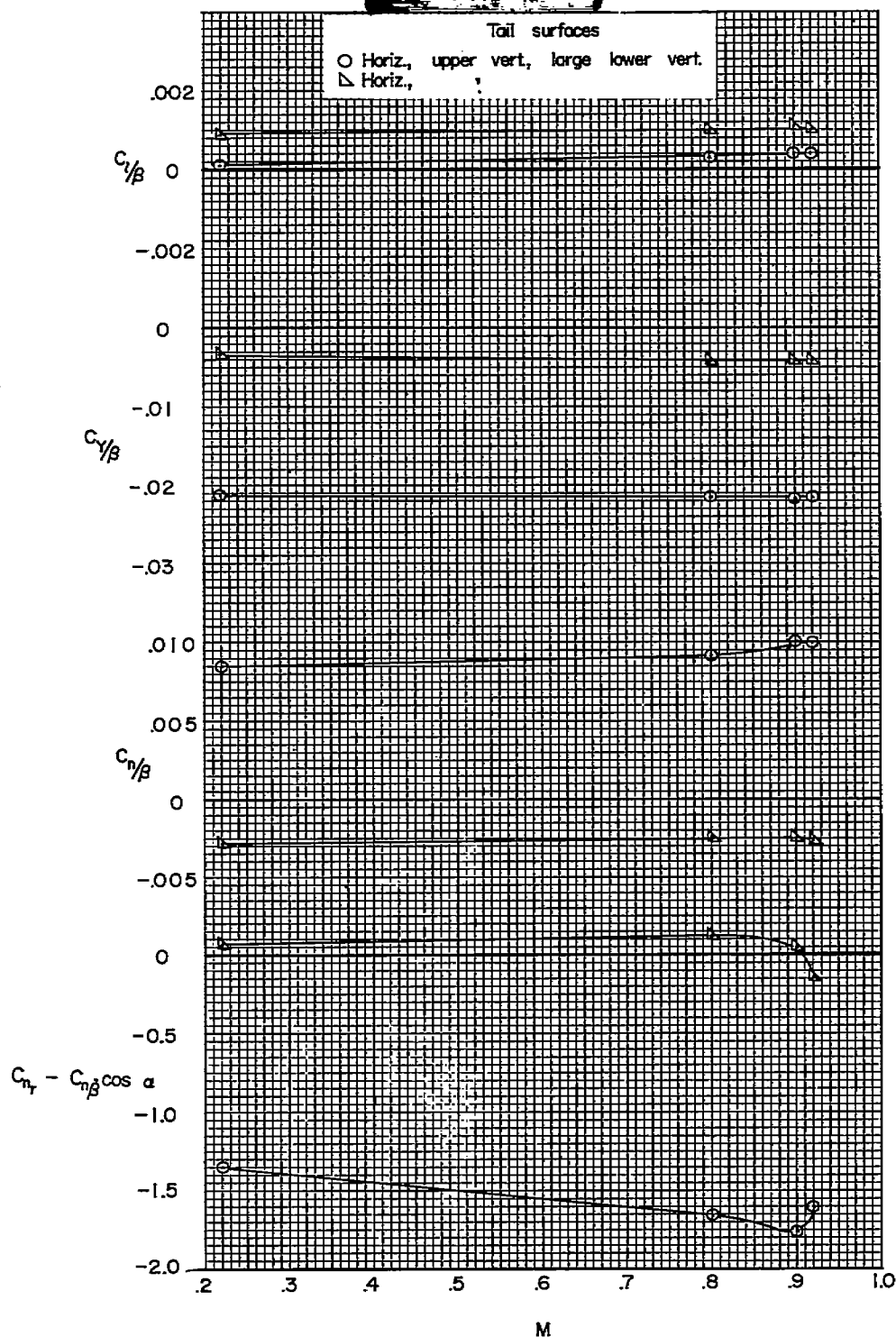


Figure 16.- Variation with Mach number of the static lateral-directional derivatives and damping in yaw; $\alpha = 0^\circ$.

NASA Technical Library



3 1176 01435 0251

